Eur. Phys. J. C 10, 499–513 (1999)
Digital Object Identifier (DOI) 10.1007/s100529900131

THE EUROPEAN PHYSICAL JOURNAL C

The $\gamma\gamma \to \gamma Z$ process at high energies and the search for virtual SUSY effects*

G.J. Gounaris[1], J. Layssac[2], P.I. Porfyriadis[1], F.M. Renard[2]

[1] Department of Theoretical Physics, Aristotle University of Thessaloniki, GR-54006, Thessaloniki, Greece
[2] Physique Mathématique et Théorique, UMR 5825, Université Montpellier II, F-34095 Montpellier Cedex 5, France

Received: 26 April 1999 / Published online: 8 September 1999

Abstract. We study the helicity amplitudes and the observables of the process $\gamma\gamma \to \gamma Z$ at high energy. As in the case of the $\gamma\gamma \to \gamma\gamma$ process studied before, the relevant diagrams in the standard model (SM) involve W, charged-quark, and lepton loops, while in SUSY we also have contributions from charginos and charged-sfermion or Higgs-loop diagrams. Above 250 GeV, the dominant SM amplitudes are themselves dominated by the W loop, and as for $\gamma\gamma \to \gamma\gamma$, they are helicity conserving and almost purely imaginary. We discuss the complementary information provided by $\gamma\gamma \to \gamma Z$ for the identification of possible nonstandard effects. This process, together with $\gamma\gamma \to \gamma\gamma$, should provide very useful information on the nature of possible new physics particles, above the threshold of their direct production.

1 Introduction

In previous papers [1,2], we have studied the process $\gamma\gamma \to \gamma\gamma$. The most striking property of this process in the standard model (SM) is that its whole set of possible helicity amplitudes is strongly dominated by just the three helicity-conserving ones, which, moreover, are almost purely imaginary. This simple property offers new possibilities for improving the search for new physics (NP) at high energy. Some of these possibilities related to $\gamma\gamma \to \gamma\gamma$ have been investigated in the aforementioned papers. We now extend this study to the process $\gamma\gamma \to \gamma Z$.

The remarkable property of the $\gamma\gamma \to \gamma\gamma$ processes mentioned above is due to the fact that the SM amplitude first appears at the one-loop level, and at high energies, it is dominated by the W-loop contribution, which mainly enhances the imaginary parts of the three-helicity nonflip amplitudes. Thus, in SM, this process is dominated by just a few almost purely imaginary helicity- conserving amplitudes. As we will see in the present work, similar properties are also valid for the process $\gamma\gamma \to \gamma Z$ studied here.

This suggests the use of $\gamma\gamma \to \gamma\gamma,\ \gamma Z$ processes as a tool for searching for types of new physics characterized by amplitudes with a substantial imaginary part that can interfere with the SM one, e.g., effects due to chargino or charged-slepton-loop diagrams above the threshold, s-channel resonance production, or new strong interactions inducing unitarity saturating contributions to the NP amplitudes.

* Partially supported by the grant CRG 971470 and by the Greek government grant PENED/95 K.A. 1795

These studies could be achieved at a future e^+e^- linear collider (LC) [3], operating as a $\gamma\gamma$ collider ($LC_{\gamma\gamma}$) whose c.m. energy may be variable and as high as 80% of the initial e^+e^- c.m. energy, by the use of the laser backscattering technique [4,5]. Polarized $\gamma\gamma$ beams can also be obtained through the use of initially polarized electron beams and lasers.

This search for NP through its virtual effects is complementary to the direct production of new particles and should help in the identification of their nature, since it avoids the model-dependent task of studying their decay modes, once they are actually produced. More explicitly, the charged-sparticle-loop contribution to $\gamma\gamma \to \gamma\gamma,\ \gamma Z$ is independent of the many parameters entering their decay modes and determining, e.g., the soft SUSY breaking and the possible R parity-violating sectors.

In the present paper, we study in detail the $\gamma\gamma \to \gamma Z$ amplitudes in the standard and SUSY models. The idea is to confirm and improve the searches for NP signatures that can be done through direct production and the measurements of the $\gamma\gamma \to \gamma\gamma$ process. The situation for such measurements should be more favorable in $\gamma\gamma \to \gamma Z$ than in $\gamma\gamma \to \gamma\gamma$, because the cross section is larger by a factor of about 6. Then, if a signal suspected in $\gamma\gamma \to \gamma\gamma$ is also seen here, the detailed properties of the SM departures, which now depend on the occurrence of the Z couplings, should allow some identification of the nature of the effect. In particular, it should help identifying the $\mathrm{SU}(2) \times \mathrm{U}(1)$ quantum numbers of the new physics particle contributing virtually.

In Sect. 2, we discuss the main properties of the W, fermion, and scalar-loop contributions at high energies, which had not been fully analyzed before. This allows us to predict the type of effects expected in case of NP con-

tributions caused by new fermion or scalar particle loops. We consider SUSY as an example of such an NP, and we discuss the physical properties of the contribution to the above amplitudes from a chargino or a charged slepton, showing how the presence of the Z coupling can distinguish them. For example, the magnitude of the contribution changes notably when passing from a gaugino-like to a higgsino-like contribution. And for an slepton loop, even changes of sign appear, when it passes from an L slepton to an R slepton case.

In Sect. 3, we study the $\gamma\gamma \to \gamma Z$ cross sections in the standard and SUSY models for various polarizations of the incoming photons. We identify the sensitivity of these cross sections to various SUSY effects, and we discuss their observability in unpolarized and polarized $\gamma\gamma$ collisions, realized through the present ideas of laser backscattering. Finally, in Sect. 4, we summarize the results and give our conclusions.

The explicit expressions for the W- [6,7] and fermion-loop [8,6] contributions to the helicity amplitudes are given in Appendix A, using the nonlinear gauge of [9]. We agree with the previous authors, apart from some slight corrections affecting the W contributions to some small helicity amplitudes. In addition, we also give the one-loop contribution induced by a single charged scalar particle. In Appendix B, simple asymptotic expressions for the helicity amplitudes are given which elucidate their physical properties at high energies.

2 An overall view of the $\gamma\gamma \to \gamma Z$ amplitudes

The invariant helicity amplitudes $F_{\lambda_1\lambda_2\lambda_3\lambda_4}(\hat{s},\hat{t},\hat{u})$ for the process $\gamma\gamma \to \gamma Z$, where λ_j are the helicities of the incoming and outgoing particles, are given in Appendix A. Altogether, there are $3 \times 2^3 = 24$ helicity amplitudes, which must of course satisfy the constraints from Bose (A.2). In SM or SUSY models, charge conjugation enforces parity invariance at the one-loop level, which implies (A.3) and allows us to express all helicity amplitudes in terms of nine analytic functions, six for transverse Z and three for longitudinal Z:

$$F_{++++}(\hat{s},\hat{t},\hat{u})\ ,\ F_{+++-}(\hat{s},\hat{t},\hat{u}), F_{++-+}(\hat{s},\hat{t},\hat{u})\ ,$$
$$F_{++--}(\hat{s},\hat{t},\hat{u})\ , F_{+-+-}(\hat{s},\hat{t},\hat{u}) = F_{+--+}(\hat{s},\hat{u},\hat{t}),$$
$$F_{+---}(\hat{s},\hat{t},\hat{u}) = F_{+-++}(\hat{s},\hat{u},\hat{t})\ , F_{+++0}(\hat{s},\hat{t},\hat{u})\ ,$$
$$F_{++-0}(\hat{s},\hat{t},\hat{u}) F_{+-+0}(\hat{s},\hat{t},\hat{u}) = F_{+--0}(\hat{s},\hat{u},\hat{t})\ .$$

In Appendix A, we reproduce the[1] W and charged-fermion contributions of [7,6,8], and we also give the contributions to these amplitudes that are due to a scalar particle loop. The essential difference between these amplitudes and those of the $\gamma\gamma \to \gamma\gamma$ case presented in [1] (apart from the obvious m_Z-dependent kinematic terms) is the appearance of longitudinal Z states and the replacement of the factor Q_x^4 by $Q_x^3 g_{Vx}^Z$ for an x-particle-loop contribution.

All results are given in terms of the standard one-loop functions B_0, C_0, and D_0, first introduced in [10]. Explicit asymptotic expressions for these functions, relevant for the $\gamma\gamma \to \gamma Z$ kinematics, are given in Appendix B. The dominant W contributions to the corresponding asymptotic helicity amplitudes are also given there; the corresponding expressions for the fermion and scalar contributions can be easily written using the presented formulae.

In the *standard model* and for $\hat{s} \gtrsim (250\text{GeV})^2$, the only nonnegligible amplitudes in both the $\gamma\gamma \to \gamma Z$ and $\gamma\gamma \to \gamma\gamma$ process are $F_{\pm\pm\pm\pm}(\hat{s},\hat{t},\hat{u})$ and $F_{\pm\mp\pm\mp}(\hat{s},\hat{t},\hat{u}) = F_{\pm\mp\mp\pm}(\hat{s},\hat{u},\hat{t})$, which turn out to be completely dominated by the W-loop contribution and almost purely imaginary. They satisfy

$$\text{Im}F^W_{\gamma\gamma\to\gamma Z} \simeq \frac{c_W}{s_W}\text{Im}F^W_{\gamma\gamma\to\gamma\gamma}\ . \tag{1}$$

The fermion-loop contribution to these same amplitudes is much smaller; its real and imaginary parts are comparable, and roughly satisfy

$$F^f_{\gamma\gamma\to\gamma Z} \simeq \frac{g^Z_{Vf}}{Q_f} F^f_{\gamma\gamma\to\gamma\gamma}\ , \tag{2}$$

where for a standard quark or lepton f,

$$g^Z_{Vf} = \frac{t_3^f - 2Q_f s_W^2}{2c_W s_W}\ . \tag{3}$$

The rest of the amplitudes turn out to be much smaller than the above dominant ones. For them, the real and imaginary parts are roughly on the same footing, as well the W- and fermion-loop contributions.

Numerical results for these amplitudes using the exact one-loop functions are presented in Fig. 1a,b, and they agree with the above expectations. Indeed, the real part of the large amplitudes $F_{\pm\pm\pm\pm}(\hat{s},\hat{t},\hat{u})$ and $F_{\pm\mp\pm\mp}(\hat{s},\hat{t},\hat{u}) = F_{\pm\mp\mp\pm}(\hat{s},\hat{u},\hat{t})$ is always more than 4(15) times smaller than the imaginary part at $\sqrt{\hat{s}} \simeq 0.3(0.6)$ TeV.

As in the $\gamma\gamma \to \gamma\gamma$ case [1], the asymptotic expressions in Appendix B are quite accurate in describing the large SM helicity amplitudes $F_{\pm\pm\pm\pm}(\hat{s},\hat{t},\hat{u})$ and $F_{\pm\mp\pm\mp}(\hat{s},\hat{t},\hat{u}) = F_{\pm\mp\mp\pm}(\hat{s},\hat{u},\hat{t})$, for the process $\gamma\gamma \to \gamma Z$ also. This is due to the fact that the double-log real contributions from (B.8, B.7) always cancel out for physical amplitudes, and the only important contributions remaining are the single-log imaginary ones. For the rest of the helicity amplitudes, all log contributions either cancel out or are strongly suppressed by $m_W^2/\hat{s}$ factors.

This confirms the fact that $\gamma\gamma \to \gamma Z$, much like $\gamma\gamma \to \gamma\gamma$ scattering, may provide a very useful tool for searching for types of NP, with largely imaginary amplitudes [2].

We have thus computed the *contributions of SUSY particles*, i.e., the contributions from a chargino or an sfermion loop.

The contribution from the lightest positively charged chargino χ_1^+ is obtained from the effective interaction (A.22) by using [11]

[1] Certain corrections are found for the W contributions to some small helicity amplitudes, when we compare our results to [7]

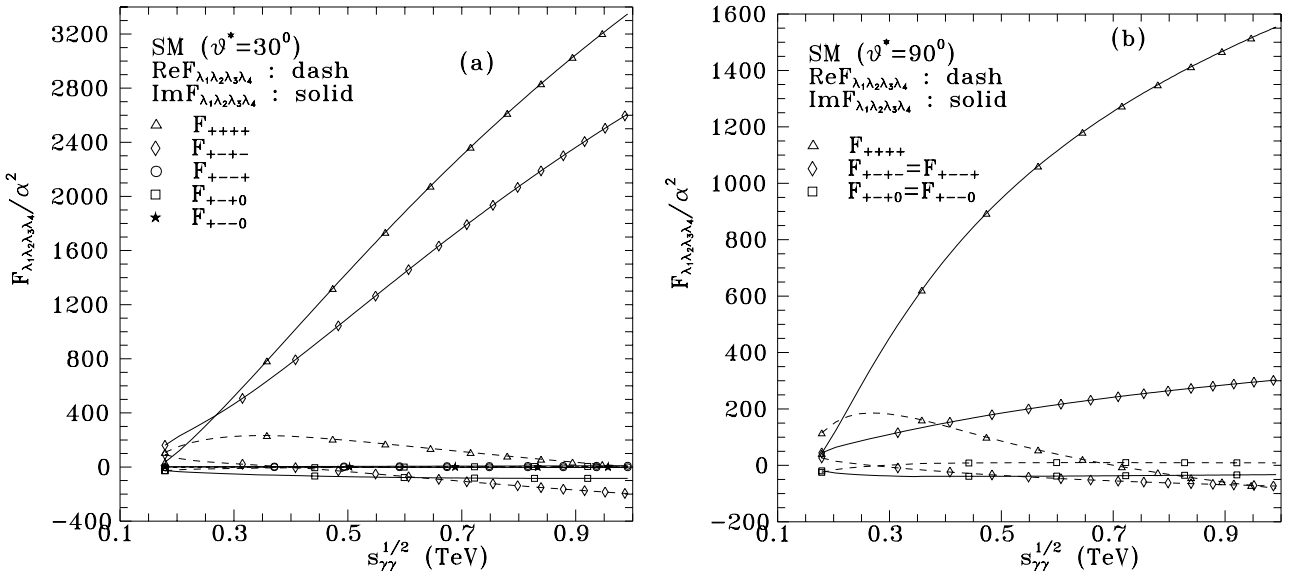

Fig. 1a,b. SM contribution to the dominant $\gamma\gamma \to \gamma Z$ helicity amplitudes at $\vartheta^* = 30^0$ and $\vartheta^* = 90^0$. All other amplitudes are predicted to be smaller or about equal to F_{+-+0} or F_{+--0}

$$g^Z_{V\chi} = \frac{1}{2c_W s_W}\left\{\frac{3}{2} - 2s^2_W + \frac{1}{4}[\cos(2\phi_L) + \cos(2\phi_R)]\right\} , \tag{4}$$

with

$$\cos(2\phi_L) = -\frac{M_2^2 - \mu^2 - 2m_W^2\cos(2\beta)}{\sqrt{(M_2^2+\mu^2+2m_W^2)^2 - 4[M_2\mu - m_W^2\sin(2\beta)]^2}} ,$$
$$\cos(2\phi_R) = -\frac{M_2^2 - \mu^2 + 2m_W^2\cos(2\beta)}{\sqrt{(M_2^2+\mu^2+2m_W^2)^2 - 4[M_2\mu - m_W^2\sin(2\beta)]^2}} , \tag{5}$$

and

$$M^2_{\chi_1^+} = \frac{1}{2}\left\{M_2^2 + \mu^2 + 2m_W^2 - \sqrt{(M_2^2+\mu^2+2m_W^2)^2 - 4\left[M_2\mu - m_W^2\sin(2\beta)\right]^2}\right\}. \tag{6}$$

Using the formulas (A.27–A.35) in Appendix A, together with the exact one-loop calculation from [12] and (4, 6), we present in Fig. 2 the results for two almost extreme situations corresponding to a light chargino of mass $M_{\chi_1^+} \simeq 95$ GeV and $\tan\beta = 2$. In the first case, the chargino nature is taken as gaugino-like by choosing (see Fig. 2a,b)

$$M_2 = 0.081 \text{ TeV} , \qquad \mu = -0.215 \text{ TeV} , \qquad g^Z_{V\chi} = 1.72 ; \tag{7}$$

while in the second case, it is taken to be higgsino-like by choosing (see Fig. 2c,d)

$$M_2 = 0.215 \text{ TeV} , \qquad \mu = -0.081 \text{ TeV} , \qquad g^Z_{V\chi} = 0.73 . \tag{8}$$

We also consider the L- and R-slepton cases, with $M_{\tilde{l}} = 0.1$ TeV, $Q_{\tilde{l}} = -1$, and

$$g^Z_{V\tilde{l}} = \frac{1}{c_W s_W}\left[t^{\tilde{l}}_3 - Q_{\tilde{l}} s^2_W\right] . \tag{9}$$

For $t^{\tilde{l}}_3 = -\frac{1}{2}$, these lead to $g^Z_{V\tilde{l}} = -0.65$ (case L), while for $t^{\tilde{l}}_3 = 0$ we find $g^Z_{V\tilde{l}} = +0.54$ (case R). As a result, a change of sign appears between L- and R-slepton contributions. The corresponding results for an slepton are derived through the use of (A.40– A.48) and presented in Fig. 3a–d.

As seen for both the cases of Fig. 2a–d and those of Fig. 3a–d, the real and imaginary parts of the fermion- or scalar-loop contributions to the $\gamma\gamma \to \gamma Z$ amplitudes above threshold are more or less on the same footing. It is also seen that immediately above the threshold, an imaginary contribution to the $F_{\pm\pm\pm\pm}(\hat{s},\hat{t},\hat{u})$ and $F_{\pm\mp\pm\mp}(\hat{s},\hat{t},\hat{u})$ $= F_{\pm\mp\mp\pm}(\hat{s},\hat{u},\hat{t})$ amplitude starts developing that can interfere with the SM contribution and produce a measurable effect. The slepton contribution is smaller than the chargino one, by a factor of about 7.

As compared to the $\gamma\gamma \to \gamma\gamma$ case, we also notice the presence of large longitudinal Z amplitudes, for both the chargino and the slepton cases. However, these are not easily observable, since they do not find a corresponding large longitudinal SM amplitude to interfere with. So in the end, they will produce very small effect.

For transverse amplitudes, as a consequence of the g^Z_{Vf}/Q_f factor, the effect in the $\gamma\gamma \to \gamma Z$ case is larger (weaker) than the $\gamma\gamma \to \gamma\gamma$ effect in the gaugino (higgsino) cases. The corresponding effect in the slepton cases is a change in sign of their contribution to $\gamma\gamma \to \gamma Z$, when passing from the L-slepton to the R-slepton case. These properties will be directly reflected in the threshold effects

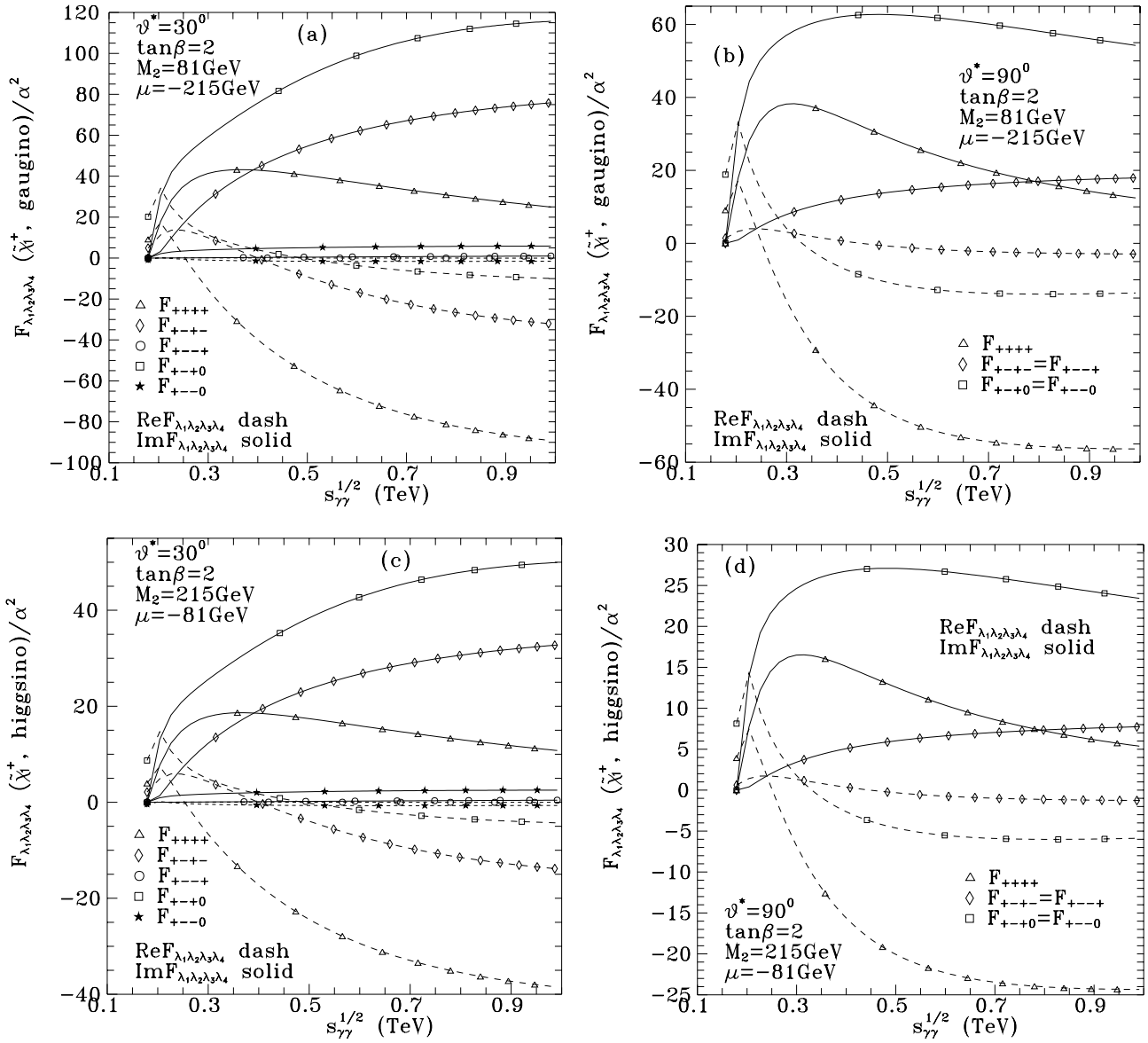

Fig. 2a–d. Chargino contribution to $\gamma\gamma \to \gamma Z$ helicity amplitudes for the gaugino (a,b) and higgsino (c,d) cases at $\vartheta^* = 30^0$ and $\vartheta^* = 90^0$. The parameters used are indicated in the figures, and $Q_{\chi_1^+} = 1$

appearing in the cross sections that we study in the next section.

3 The $\gamma\gamma \to \gamma Z$ cross sections

We next explore the possibility of using polarized or unpolarized $\gamma\gamma$ collisions in an LC operated in the $\gamma\gamma$ mode, through laser backscattering and the procedure described in [13,2]. The assumption of parity invariance leads to the following form for the $\gamma\gamma \to \gamma Z$ cross section (note the factor 2 due to the presence of a nonsymmetric final state; compare with the $\gamma\gamma \to \gamma\gamma$ case):

$$\frac{\mathrm{d}\sigma}{\mathrm{d}\tau \mathrm{d}\cos\vartheta^*}$$

$$= \frac{\mathrm{d}\bar{L}_{\gamma\gamma}}{\mathrm{d}\tau}\Bigg\{ \frac{\mathrm{d}\bar{\sigma}_0}{\mathrm{d}\cos\vartheta^*} + \langle\xi_2\xi_2'\rangle \frac{\mathrm{d}\bar{\sigma}_{22}}{\mathrm{d}\cos\vartheta^*}$$
$$+\langle\xi_3\rangle \cos 2\phi \frac{\mathrm{d}\bar{\sigma}_3}{\mathrm{d}\cos\vartheta^*} + \langle\xi_3'\rangle \cos 2\phi' \frac{\mathrm{d}\bar{\sigma}_3'}{\mathrm{d}\cos\vartheta^*}$$
$$+\langle\xi_3\xi_3'\rangle \left[\frac{\mathrm{d}\bar{\sigma}_{33}}{\mathrm{d}\cos\vartheta^*}\cos 2(\phi+\phi') + \frac{\mathrm{d}\bar{\sigma}_{33}'}{\mathrm{d}\cos\vartheta^*}\cos 2(\phi-\phi')\right]$$
$$+\langle\xi_2\xi_3'\rangle \sin 2\phi' \frac{\mathrm{d}\bar{\sigma}_{23}}{\mathrm{d}\cos\vartheta^*} - \langle\xi_3\xi_2'\rangle \sin 2\phi \frac{\mathrm{d}\bar{\sigma}_{23}'}{\mathrm{d}\cos\vartheta^*}\Bigg\} \ , \quad (10)$$

where

$$\frac{\mathrm{d}\bar{\sigma}_0}{\mathrm{d}\cos\vartheta^*} = \left(\frac{\beta_Z}{64\pi\hat{s}}\right) \sum_{\lambda_3\lambda_4} [|F_{++\lambda_3\lambda_4}|^2 + |F_{+-\lambda_3\lambda_4}|^2] \ , (11)$$

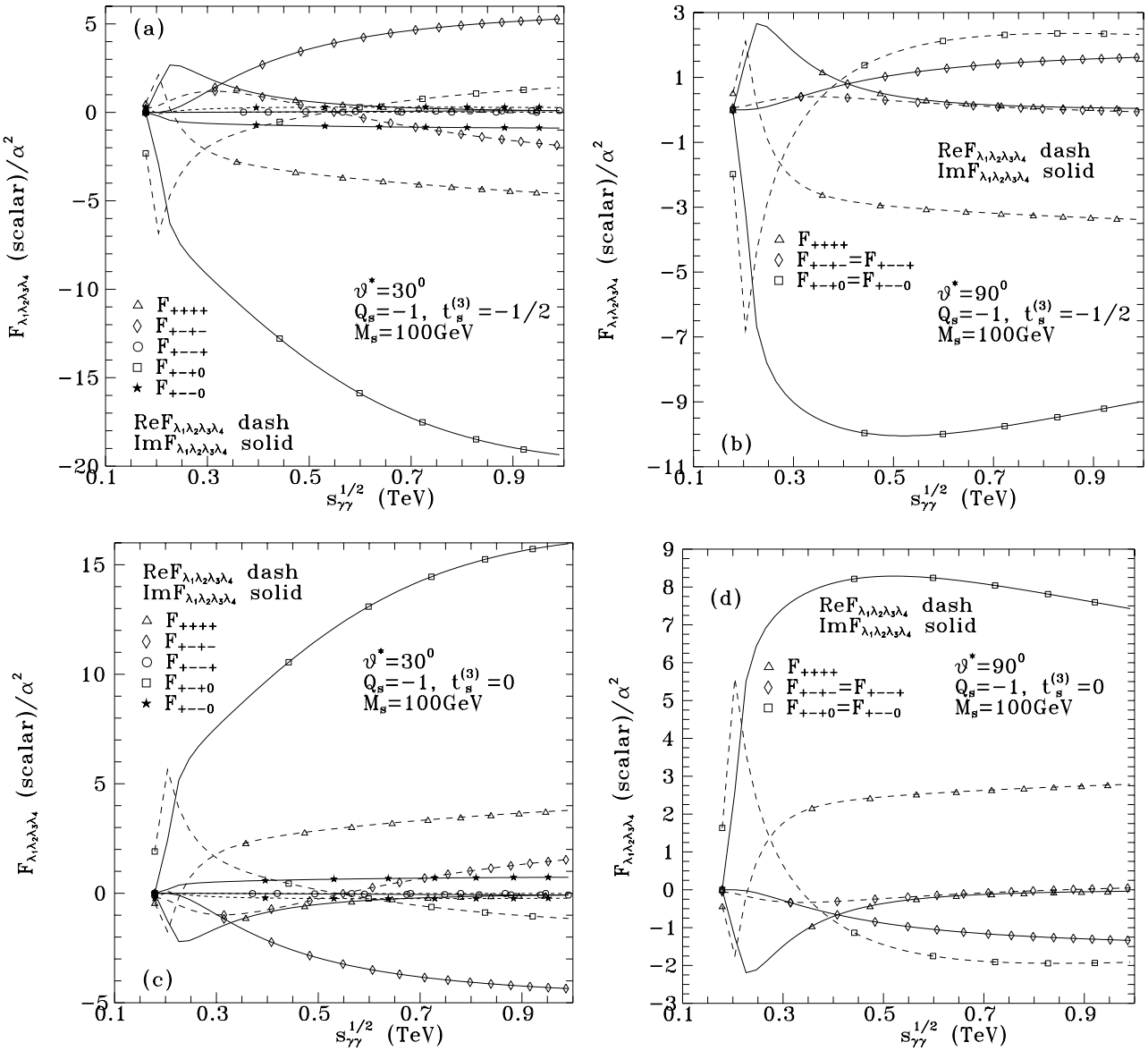

Fig. 3a–d. Contribution to $\gamma\gamma \to \gamma Z$ helicity amplitudes from an isodoublet (a,b) and an isosinglet (c,d) slepton at $\vartheta^* = 30^0$ and $\vartheta^* = 90^0$. The parameters used are indicated in the figures, and the slepton mass is taken as $M_{\tilde{l}} = M_s = 100$ GeV

$$\frac{\mathrm{d}\bar{\sigma}_{22}}{\mathrm{d}\cos\vartheta^*} = \left(\frac{\beta_Z}{64\pi\hat{s}}\right) \sum_{\lambda_3\lambda_4} [|F_{++\lambda_3\lambda_4}|^2 - |F_{+-\lambda_3\lambda_4}|^2] \ , \quad (12)$$

$$\frac{\mathrm{d}\bar{\sigma}_3}{\mathrm{d}\cos\vartheta^*} = \left(\frac{-\beta_Z}{32\pi\hat{s}}\right) \sum_{\lambda_3\lambda_4} \mathrm{Re}[F_{++\lambda_3\lambda_4} F^*_{-+\lambda_3\lambda_4}] \ , \quad (13)$$

$$\frac{\mathrm{d}\bar{\sigma}'_3}{\mathrm{d}\cos\vartheta^*} = \left(\frac{-\beta_Z}{32\pi\hat{s}}\right) \sum_{\lambda_3\lambda_4} \mathrm{Re}[F_{++\lambda_3\lambda_4} F^*_{+-\lambda_3\lambda_4}] \ , \quad (14)$$

$$\frac{\mathrm{d}\bar{\sigma}_{33}}{\mathrm{d}\cos\vartheta^*} = \left(\frac{\beta_Z}{64\pi\hat{s}}\right) \sum_{\lambda_3\lambda_4} \mathrm{Re}[F_{+-\lambda_3\lambda_4} F^*_{-+\lambda_3\lambda_4}] \ , \quad (15)$$

$$\frac{\mathrm{d}\bar{\sigma}'_{33}}{\mathrm{d}\cos\vartheta^*} = \left(\frac{\beta_Z}{64\pi\hat{s}}\right) \sum_{\lambda_3\lambda_4} \mathrm{Re}[F_{++\lambda_3\lambda_4} F^*_{--\lambda_3\lambda_4}] \ , \quad (16)$$

$$\frac{\mathrm{d}\bar{\sigma}_{23}}{\mathrm{d}\cos\vartheta^*} = \left(\frac{\beta_Z}{32\pi\hat{s}}\right) \sum_{\lambda_3\lambda_4} \mathrm{Im}[F_{++\lambda_3\lambda_4} F^*_{+-\lambda_3\lambda_4}] \ , \quad (17)$$

$$\frac{\mathrm{d}\bar{\sigma}'_{23}}{\mathrm{d}\cos\vartheta^*} = \left(\frac{\beta_Z}{32\pi\hat{s}}\right) \sum_{\lambda_3\lambda_4} \mathrm{Im}[F_{++\lambda_3\lambda_4} F^*_{-+\lambda_3\lambda_4}] \ , \quad (18)$$

are expressed in terms of the $\gamma\gamma \to \gamma Z$ amplitudes given in Appendix A. In (11–18), $\beta_Z = 1 - m_Z^2/\hat{s}$ is the Z velocity in the $\gamma\gamma$ rest frame, while ϑ^* is the scattering angle, and $\tau \equiv s_{\gamma\gamma}/s_{ee}$. Note that $\mathrm{d}\bar{\sigma}_0/\mathrm{d}\cos\vartheta^*$ is the unpolarized cross section and that it is the only $\bar{\sigma}_j$ quantity which is positive definite. We also note that $\mathrm{d}\bar{\sigma}_j/\mathrm{d}\cos\vartheta^*$ are forward–backward symmetric, except those below, which

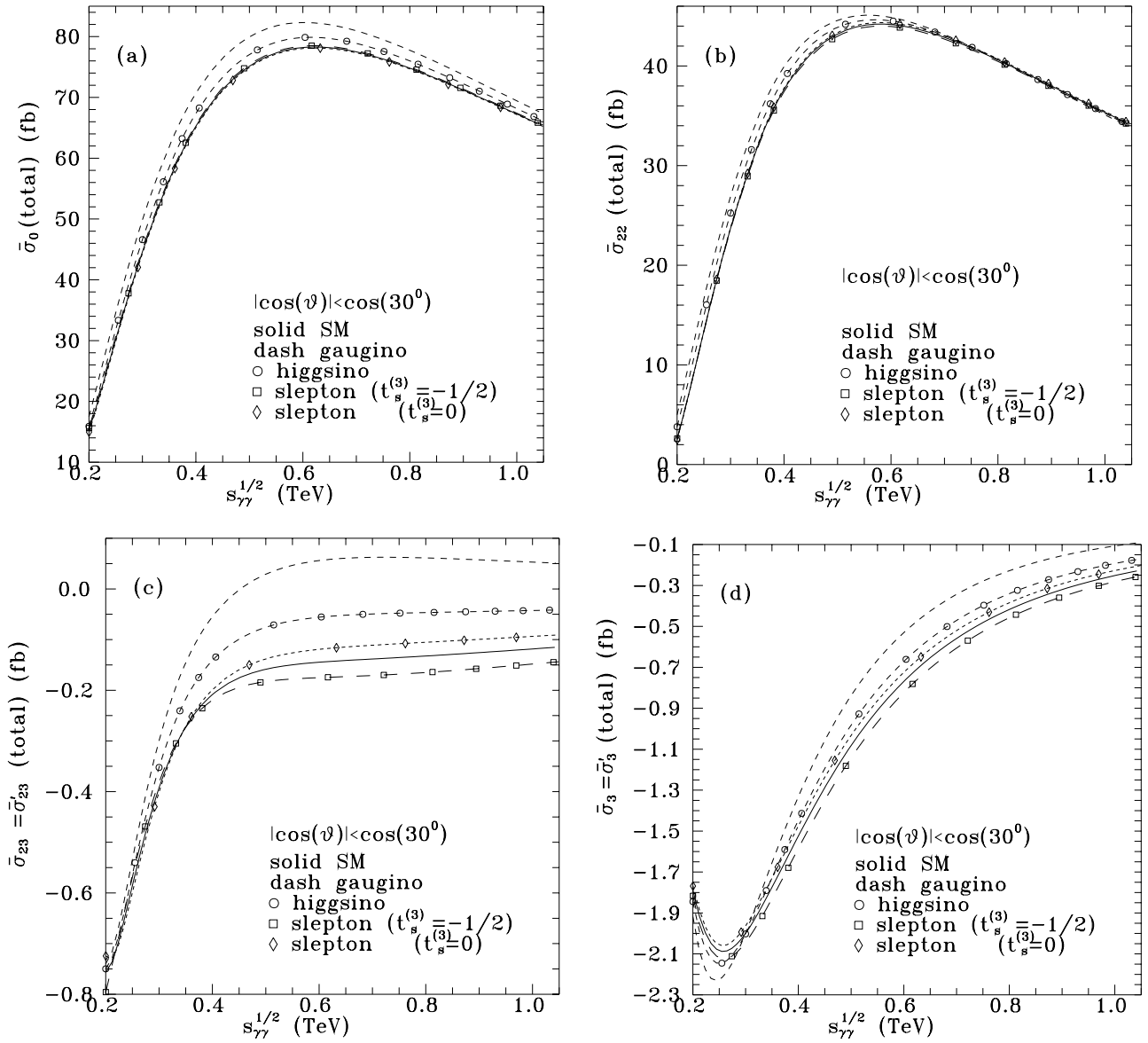

Fig. 4a–d. $\bar\sigma_0$, $\bar\sigma_{22}$, $\bar\sigma_{23}=\bar\sigma'_{23}$, and $\bar\sigma_3=\bar\sigma'_3$ for SM (solid) and in the presence of a chargino (dashes, dashes–circles) or a charged-slepton (box, rhombus) contribution, with the same parameters as in Fig. 2 and Fig. 3, respectively

satisfy

$$\left.\frac{\mathrm{d}\bar\sigma'_3}{\mathrm{d}\cos\vartheta^*}\right|_{\vartheta^*} = \left.\frac{\mathrm{d}\bar\sigma_3}{\mathrm{d}\cos\vartheta^*}\right|_{\pi-\vartheta^*}, \tag{19}$$

$$\left.\frac{\mathrm{d}\bar\sigma'_{23}}{\mathrm{d}\cos\vartheta^*}\right|_{\vartheta^*} = \left.\frac{\mathrm{d}\bar\sigma_{23}}{\mathrm{d}\cos\vartheta^*}\right|_{\pi-\vartheta^*}. \tag{20}$$

The results for the cross sections $\bar\sigma_j$, integrated in the range $30^0 \le \vartheta^* \le 150^0$, are given in Fig. 4a–f, for the standard model as well as for the cases of including the contributions from a single chargino or a single charged slepton with mass of about 95 or 100 GeV respectively.

As seen in Fig. 4a, the effects in the unpolarized cross section $\bar\sigma_0$ are consistent with those expected from the dominant imaginary amplitudes quoted in the previous section. In more detail, the (gaugino, higgsino) effects are of the order of (10, 5)%, respectively, while the slepton ones are an order of magnitude smaller.

The *relative* (NP versus SM) effects are somewhat reduced in $\bar\sigma_{22}$, but they are largely enhanced in the other $\bar\sigma_j$ cross sections; (compare Fig. 4b with Fig. 4c–f.). However, most of the latter cross sections have small absolute values, making them unlikely to be observed. Only $\bar\sigma_3$ and $\bar\sigma_{33}$ are of the order of a few fb. The SUSY effects are here notably enhanced as compared to the SM contributions, reaching the 25% level in some cases. Particularly striking is the SUSY effect for $\bar\sigma_{33}$ and $\bar\sigma'_{33}$ near but above threshold. For $\bar\sigma'_{33}$, such a behavior also occurred in the $\gamma\gamma \to \gamma\gamma$ case [1], and it may be useful for disentangling of the various SUSY examples.

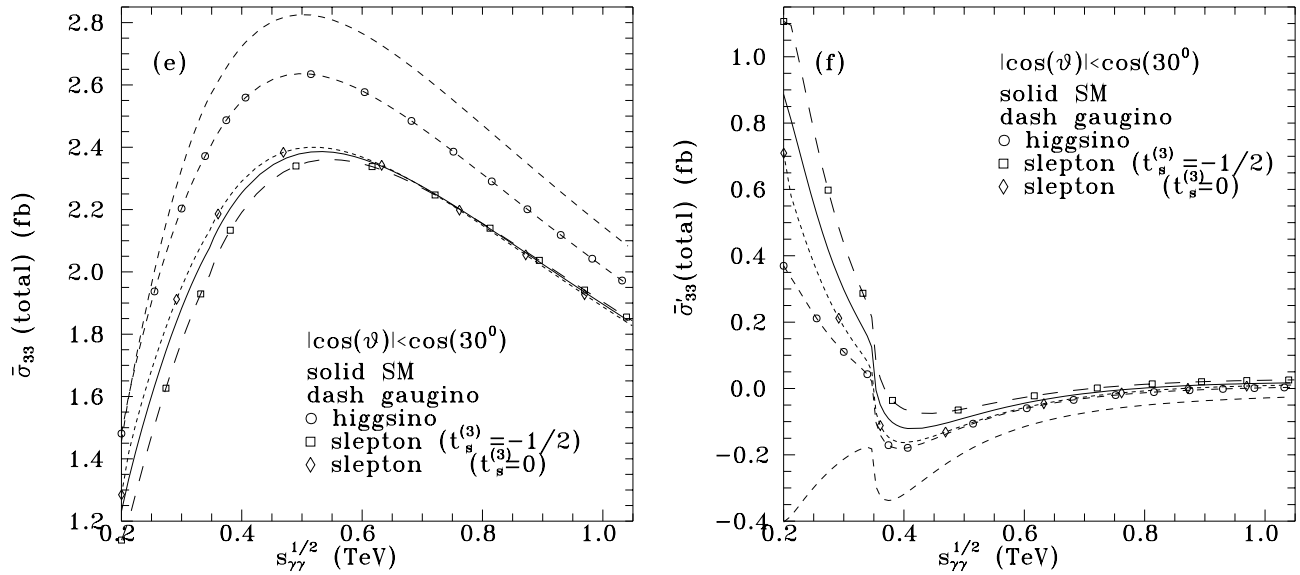

Fig. 4e,f. $\bar{\sigma}_{33}$ and $\bar{\sigma}'_{33}$ for SM (solid) and in the presence of a chargino (dashes, dashes–circles) or a charged-slepton (box, rhombus) contribution, with the same parameters as in Fig. 2 and Fig. 3, respectively

In the present case, the option to select longitudinal polarization for the outgoing Z is also available. In this case, remarkable SUSY effects, strongly dependent on the type of particle running along the loop, are generated. However, the absolute values of the related cross sections are unfortunately less than 1 fb, rendering these effects unobservable. See Fig. 5a–c where $\bar{\sigma}_0(Z_L)$, $\bar{\sigma}_{22}(Z_L)$ and $\bar{\sigma}_{33}(Z_L)$ are presented; the other ones are less than 0.1 fb.

The angular distributions of the various $\mathrm{d}\bar{\sigma}_j/\mathrm{d}\cos\vartheta^*$ are illustrated for $\sqrt{s} = 0.4$ TeV in Fig. 6a–f. Restricting the discussion to those cross sections whose absolute values are larger than 1 fb; one observes that forward–backward peaks arise only for $\mathrm{d}\bar{\sigma}_0/\mathrm{d}\cos\vartheta^*$. Among the rest, the most interesting ones are $\mathrm{d}\bar{\sigma}_{22}/\mathrm{d}\cos\vartheta^*$, $\mathrm{d}\bar{\sigma}_3/\mathrm{d}\cos\vartheta^*$ (note (19)), and $\mathrm{d}\bar{\sigma}_{33}/\mathrm{d}\cos\vartheta^*$; which in fact have a forward deep. At a weaker level, a similar result is true for $\gamma\gamma \to \gamma\gamma$, where of course all cross sections are forward–backward symmetric (but no figures are shown in [1]). Figure 6a–f also show that SUSY effects often appear mostly pronounced at large angles.

To get a feeling of the observability of the various quantities $\bar{\sigma}_j$ appearing in (10), we next turn to the experimental aspects of the $\gamma\gamma$ collision realized through laser backscattering [3,4]. The quantity $\mathrm{d}\bar{L}_{\gamma\gamma}/\mathrm{d}\tau$ in (10) describes the photon–photon luminosity-per-unit e^-e^+ flux, in an LC operated in the $\gamma\gamma$ mode [4]. The Stokes parameters ξ_2, ξ_3 and the polarization angle ϕ in (10) determine the normalized helicity density matrix of one of the backscattered photons $\rho^{BN}_{\lambda\bar{\lambda}}$ through the formalism described in Appendix B of [1]; compare the equation (B4) of [1] and [13]. The corresponding parameters for the other backscattered photon are denoted by a prime. The numerical expectations for $\mathrm{d}\bar{L}_{\gamma\gamma}/\mathrm{d}\tau$, $\langle\xi_j\rangle$, $\langle\xi'_j\rangle$, and $\langle\xi_i\xi'_j\rangle$ are given in Appendix B and Fig. 4 of [1]. To estimate the expected number of events, one should multiply the cross sections in (10) by the e^+e^- luminosity $\mathcal{L}_{ee}$, whose presently contemplated value for the LC project is $\mathcal{L}_{ee} \simeq 500 - 1000$ fb^{-1} per one or two years of running in, e.g., the high-luminosity TESLA mode at energies of 350–800 GeV [3].

We next turn to the expected statistical accuracies for the various $\bar{\sigma}_j$. The relative uncertainty for the unpolarized cross section $[\bar{\sigma}_0(\langle\cos\vartheta^*\rangle)]$, calculated by integrating the respective differential cross section over a certain reduced-energy bin $\Delta\tau$ and an angular bin $\Delta\cos\vartheta^*$, is:

$$\frac{\delta\left[\bar{\sigma}_0(\langle\cos\vartheta^*\rangle)\right]}{\left[\bar{\sigma}_0(\langle\cos\vartheta^*\rangle)\right]} = \left[\mathcal{L}_{ee}(\Delta\tau)\,(\Delta\cos\vartheta^*)\left(\frac{\mathrm{d}\bar{L}_{\gamma\gamma}}{\mathrm{d}\tau}\right)\left(\frac{\mathrm{d}\bar{\sigma}_0}{\mathrm{d}\cos\vartheta^*}\right)\right]^{-\frac{1}{2}}. \quad (21)$$

For the other cross sections, for whose measurement we need various combinations of longitudinal $e^{\pm}$, and longitudinal and transverse laser polarizations, we perform an analysis similar to the one in Sect. 3 of [1]. For simplicity, we define

$$R_j\left(\langle\cos\vartheta^*\rangle\right) \equiv \frac{\left[\bar{\sigma}_{ij}\left(\langle\cos\vartheta^*\rangle\right)\right]}{\left[\bar{\sigma}_0\left(\langle\cos\vartheta^*\rangle\right)\right]_{\mathrm{SM}}}\,. \quad (22)$$

Then, the absolute uncertainties $\delta[\bar{\sigma}_{ij}(\langle\cos\vartheta^*\rangle)]$ satisfy

$$\delta R_j(\langle\cos\vartheta^*\rangle) = \frac{\delta[\bar{\sigma}_{ij}(\langle\cos\vartheta^*\rangle)]}{[\bar{\sigma}_0(\langle\cos\vartheta^*\rangle)]_{\mathrm{SM}}} = \frac{1}{c_j}\left[\mathcal{L}_{ee}\,(\Delta\tau)\,(\Delta\cos\vartheta^*)\left(\frac{\mathrm{d}\bar{L}_{\gamma\gamma}}{\mathrm{d}\tau}\right)\left(\frac{\mathrm{d}\bar{\sigma}_0}{\mathrm{d}\cos\vartheta^*}\right)\right]^{-\frac{1}{2}}, \quad (23)$$

where $c_j = \sqrt{2}\langle\xi_2\xi'_2\rangle$, $\sqrt{2}\langle\xi_3\rangle$, $\langle\xi_3\xi'_3\rangle$, and $\sqrt{2}\langle\xi_2\xi'_3\rangle$, for R_{22}, R_3, (R_{33} or R'_{33}), (R_{23}, and R'_{23}), respectively.

To estimate these, we take the numerical values for the photon spectra and polarization degrees given in Appendix B and Fig. 4 of [1]. For the e^+e^- luminosity, we assume 1000 fb^{-1}. Then, using bins of the order of $\Delta\tau \simeq 0.4$,

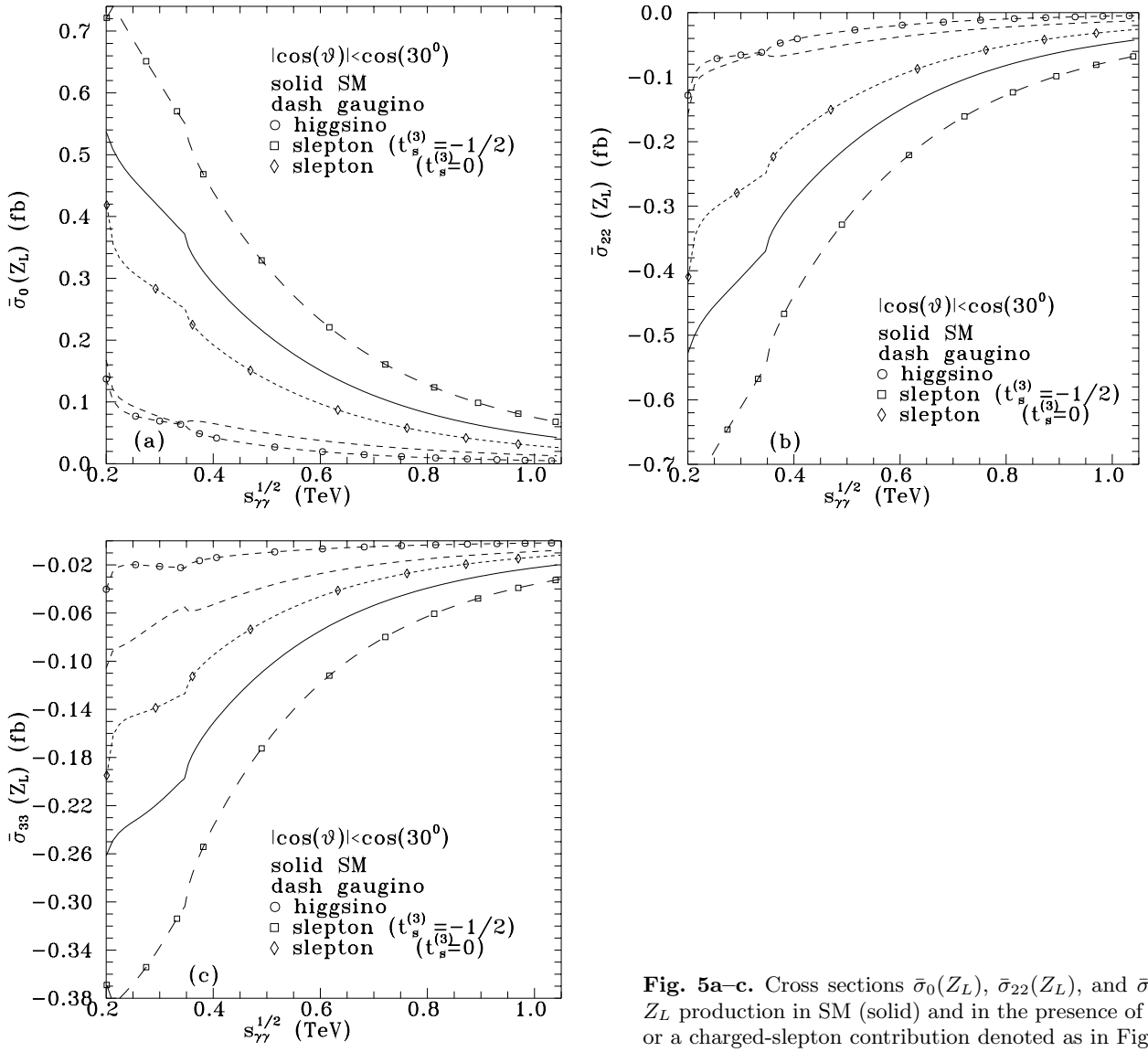

Fig. 5a–c. Cross sections $\bar{\sigma}_0(Z_L)$, $\bar{\sigma}_{22}(Z_L)$, and $\bar{\sigma}_{33}(Z_L)$ for Z_L production in SM (solid) and in the presence of a chargino or a charged-slepton contribution denoted as in Fig. 4

$\Delta \cos\vartheta^* \simeq 1$, and $\mathrm{d}\bar{L}_{\gamma\gamma}/\mathrm{d}\tau \gtrsim 1$, as well as an unpolarized differential cross section of the order of 30 fb (see Fig. 6a), one obtains a relative uncertainty of the order of 1%, for the unpolarized cross section in (21).

For the ratios R_j defined in (22), the factor $1/c_j$ will increase the absolute uncertainty in (23). According to Figs. 4 and 5 of [1], this factor depends strongly on the backscattering configurations and on the reduced-energy range, which can easily vary between 1 and 10. But if the kinematic range to be studied is known, then the backscattering configuration can be tuned to optimize the flux spectrum. Thus, for the time being, we can roughly conclude that the accuracy at which the ratios R_j can be measured should lie between 1 and 10%. This means that it is reasonable to expect an absolute uncertainty of the order of 0.3 fb for $\mathrm{d}\bar{\sigma}_0/\mathrm{d}\cos\vartheta^*$ at large angles, and something in the range (0.3–3) fb for the other $\mathrm{d}\bar{\sigma}_{ij}/\mathrm{d}\cos\vartheta^*$.

These values have to be compared with the NP effects expected on the corresponding observables. Thus, from Figs. 4 and 6, one sees that the unpolarized integrated cross section should be very sensitive to chargino effects, this sensitivity characterized by a statistical significance notably increased as compared with the $\gamma\gamma \to \gamma\gamma$ case (up to 10 SD instead of 3 SD, if the chargino is in the 100 GeV mass range). For slepton searches, the situation in $\gamma\gamma \to \gamma Z$ is similar to the one in $\gamma\gamma \to \gamma\gamma$, because of the small Z–slepton couplings.

The illustrations given in the present paper are for a chargino or slepton in the 100 GeV mass range. For higher masses, the relative merits of the $\gamma\gamma \to \gamma Z$ and $\gamma\gamma \to \gamma\gamma$ processes[2] remain about the same. We expect, therefore, that $\gamma\gamma \to \gamma Z$ should be very helpful for sparticle searches with a mass up to 300 GeV. As a final remark, we recall that in $\gamma\gamma \to \gamma\gamma$, if several SUSY particles exist within a given mass range, then their effects are all positive and cumulate in $\bar{\sigma}_0$. This is not necessarily the case in $\gamma\gamma \to$

[2] In [1] we gave an illustration of sparticles at 250 GeV in the $\gamma\gamma \to \gamma\gamma$ case

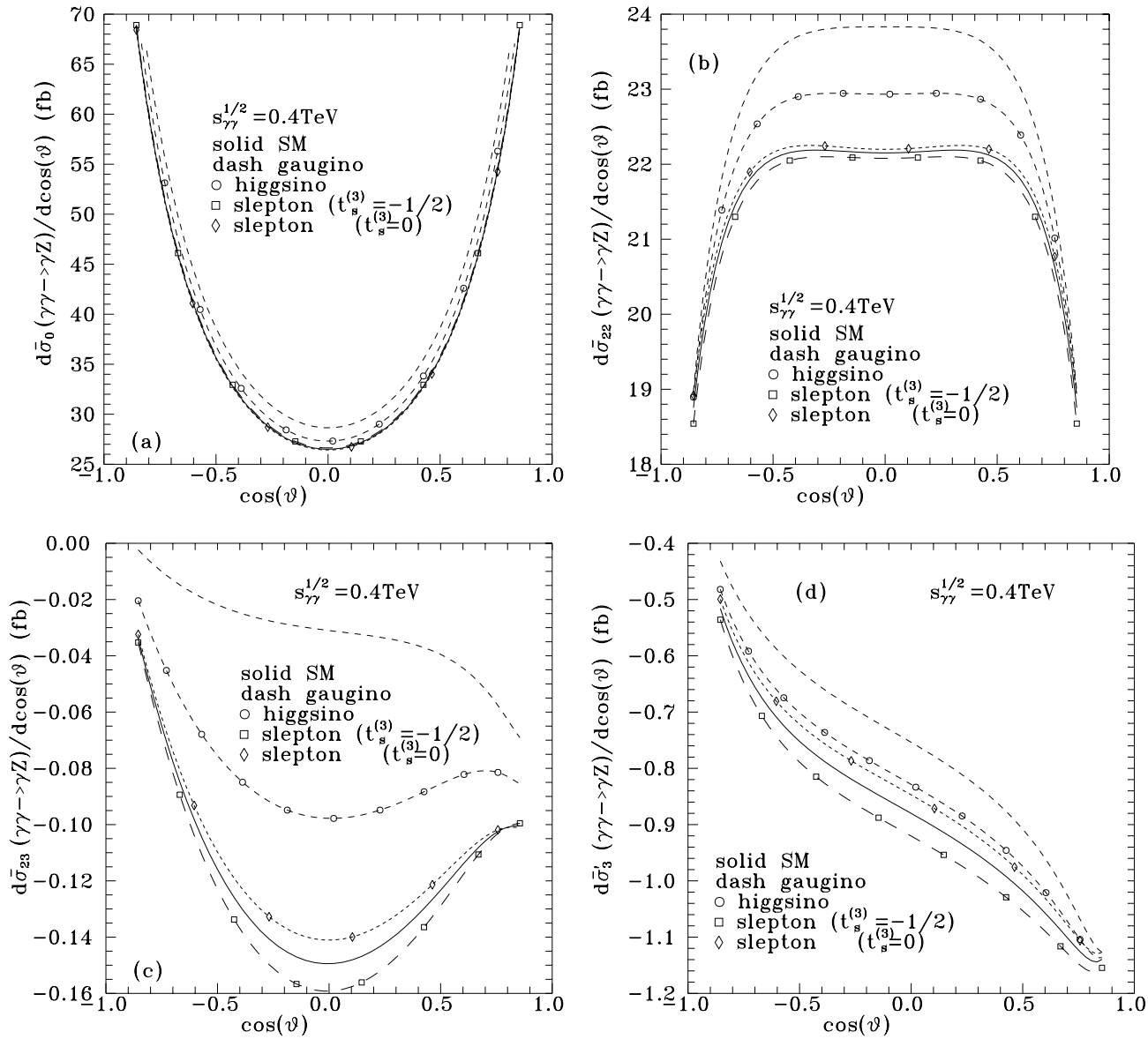

Fig. 6a–d. Angular distributions for $d\bar{\sigma}_0/d\cos\vartheta^*$, $d\bar{\sigma}_{22}/d\cos\vartheta^*$, $d\bar{\sigma}_{23}/d\cos\vartheta^*$, and $d\bar{\sigma}'_3/d\cos\vartheta^*$

γZ, because the g_{Vx}^Z can have different signs, as we have seen in Sect. 2.

4 Conclusions

In this paper, we have extended our previous analysis of the helicity amplitudes and observables in the process $\gamma\gamma \to \gamma\gamma$ at high energies to the $\gamma\gamma \to \gamma Z$ case.

It appears that both processes share the spectacular property that in the SM and at energies above 0.25 TeV, only three independent helicity-conserving amplitudes are important, which, moreover, are almost purely imaginary. This is exactly what would have been predicted about 30 years ago, on the basis of vector meson dominance and Pomeron exchange. These three amplitudes are $F_{\pm\pm\pm\pm}(\hat{s},\hat{t},\hat{u})$ and $F_{\pm\mp\pm\mp}(\hat{s},\hat{t},\hat{u}) = F_{\pm\mp\mp\pm}(\hat{s},\hat{u},\hat{t})$. Thus the $\gamma\gamma \to \gamma\gamma$ and $\gamma\gamma \to \gamma Z$ processes should be excellent tools for searching for virtual new physics contributions characterized by important imaginary contributions. This means that they should very helpful in the identification of the nature of nearby new particles, which can also be directly excited. But they should not be of much use for studying high-scale NP effects described by effective Lagrangians, which naturally lead to real amplitudes.

This has been illustrated for the particular SUSY cases of a single chargino or charged-slepton contribution. Clear threshold effects in the various observables appear, because of the interference of the imaginary parts of the SUSY amplitudes with the SM ones. These contributions depend, of course, on the mass and quantum numbers of the SUSY partners, but are independent of the many model-dependent parameters entering their decay modes, contrary to the case of direct SUSY particle production.

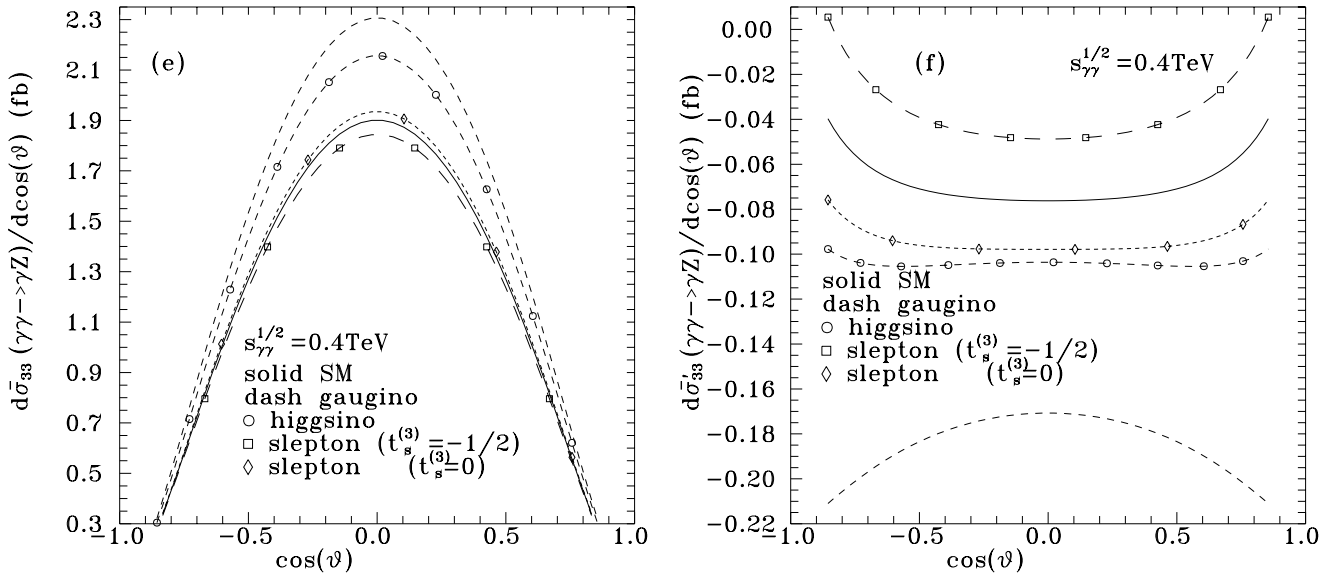

Fig. 6e,f. Angular distributions for $\mathrm{d}\bar{\sigma}_{33}/\mathrm{d}\cos\vartheta^*$ and $\mathrm{d}\bar{\sigma}'_{33}/\mathrm{d}\cos\vartheta^*$

Thus, the study of the $\gamma\gamma \to \gamma\gamma,\ \gamma Z$ cross sections should offer complementary information to that obtained from direct SUSY production cross sections. We have indeed found that the unpolarized $\gamma\gamma \to \gamma\gamma,\ \gamma Z$ cross sections $\bar{\sigma}_0$ are most sensitive to a chargino-loop contribution. For a light chargino, the signal is, at most, 3 to 4 SD in $\gamma\gamma \to \gamma\gamma$, while it can reach 10 SD in the $\gamma\gamma \to \gamma Z$ case. For a single charged slepton with a 100 GeV mass, we have found that the corresponding effect on $\bar{\sigma}_0$ is an order of magnitude smaller. Angular distributions are most sensitive at large angles ($|\cos\theta^*| < 0.5$) in both cases. Polarization should allow one to test the nature of the particles involved in the loop. There are eight different observables in $\gamma\gamma \to \gamma Z$, and six in $\gamma\gamma \to \gamma\gamma$. Only five of them ($\bar{\sigma}_0$, $\bar{\sigma}_{22}$, $\bar{\sigma}_3$, $\bar{\sigma}_{33}$, and $\bar{\sigma}'_{33}$), will be able to be measured with sufficient accuracy to allow checks of the global picture. This requires an optimization of the laser backscattering procedure, however.

The comparison of the situations in $\gamma\gamma \to \gamma\gamma$ and $\gamma\gamma \to \gamma Z$ is very instructive. It is first important to notice that in $\gamma\gamma \to \gamma\gamma$, both the charged-fermion and the charged-scalar particle loops *increase* the SM prediction for $\bar{\sigma}_0$. If, as seems quite plausible, a chargino, as well as all six charged sleptons and $\tilde{t}_1$, lie in the 100–250 GeV mass range, then a clear signal will be seen in $\bar{\sigma}_0(\gamma\gamma \to \gamma\gamma)$. The study of $\gamma\gamma \to \gamma Z$, including also polarization effects, should then give information on the origin of the signal.

A similar type of effects could also appear for other virtual NP contributions of fermionic or scalar nature, e.g., heavy fermions, technifermions, charged Higgses, pseudogoldstone bosons, or even heavy charged-vector bosons. In the $\gamma\gamma \to \gamma\gamma$ case, the effect is controlled only by the electric charge, while in $\gamma\gamma \to \gamma Z$, the g^Z_{Vx} coupling also enters in. There exist other process of this type, namely $\gamma\gamma \to ZZ$ and $\gamma\gamma \to HH,\ HZ$, which receive SM contributions only at one-loop, and could be equally interesting for NP searches. However, they are essentially controlled by the properties of the Higgs sector, and deserve separate studies, which are in progress.

In any case, it appears to us that $\gamma\gamma \to \gamma\gamma,\ \gamma Z$ are very clean processes which should supply excellent tools for NP searches, and should add to the interest in providing for the eventual realization of the $\gamma\gamma$ mode in the high-energy LC colliders.

Appendix A: the $\gamma\gamma \to \gamma Z$ amplitudes in SM and SUSY

The invariant helicity amplitudes for the process

$$\gamma(p_1,\lambda_1)\gamma(p_2,\lambda_2) \to \gamma(p_3,\lambda_3)Z(p_4,\lambda_4) \qquad \text{(A.1)}$$

are denoted as[3] $F_{\lambda_1\lambda_2\lambda_3\lambda_4}(\hat{s},\hat{t},\hat{u})$, where the momenta and helicities of the incoming and outgoing photons are indicated in parentheses, and $\hat{s}=(p_1+p_2)^2$, $\hat{t}=(p_1-p_3)^2$, $\hat{u}=(p_1-p_4)^2$. Bose statistics demands

$$F_{\lambda_1\lambda_2\lambda_3\lambda_4}(\hat{s},\hat{t},\hat{u}) = F_{\lambda_2\lambda_1\lambda_3\lambda_4}(\hat{s},\hat{u},\hat{t})(-1)^{1-\lambda_4}\ , \quad \text{(A.2)}$$

while if parity invariance also holds, we get the additional constraint

$$F_{\lambda_1\lambda_2\lambda_3\lambda_4}(\hat{s},\hat{t},\hat{u}) = F_{-\lambda_1-\lambda_2-\lambda_3-\lambda_4}(\hat{s},\hat{t},\hat{u})(-1)^{1-\lambda_4}. \quad \text{(A.3)}$$

As a result, the 24 helicity amplitudes may be expressed in terms of just the 9 amplitudes

$$F_{++++}(\hat{s},\hat{t},\hat{u})\ ,\ F_{+++-}(\hat{s},\hat{t},\hat{u}), F_{++-+}(\hat{s},\hat{t},\hat{u})\ ,$$
$$F_{++--}(\hat{s},\hat{t},\hat{u})\ , F_{+-+-}(\hat{s},\hat{t},\hat{u}) = F_{+--+}(\hat{s},\hat{u},\hat{t}),$$
$$F_{+---}(\hat{s},\hat{t},\hat{u}) = F_{+-++}(\hat{s},\hat{u},\hat{t})\ , F_{+++0}(\hat{s},\hat{t},\hat{u})\ ,$$
$$F_{++-0}(\hat{s},\hat{t},\hat{u})F_{+-+0}(\hat{s},\hat{t},\hat{u}) = F_{+--0}(\hat{s},\hat{u},\hat{t})\ .$$

[3] Their sign is related to the sign of the S matrix through $S_{\lambda_1\lambda_2\lambda_3\lambda_4} = 1 + \mathrm{i}(2\pi)^4\delta(p_f-p_i)F_{\lambda_1\lambda_2\lambda_3\lambda_4}$. We use the Jacob–Wick convention

There are three different forms of contributions to these amplitudes arising from W, fermion, or scalar particle loops. To express them economically, we use the notation of [14] for the B_0, C_0 and D_0 one-loop functions first defined by Passarino and Veltman [10], and we introduce the shorthand writing

$$B_0(\hat{s}) \equiv B_0(\hat{s}; m, m) \ , \tag{A.4}$$
$$C_0(\hat{s}) \equiv C_0(12) = C_0(0, 0, \hat{s}; m, m, m) \ , \tag{A.5}$$

and

$$B_Z(\hat{s}) \equiv B_0(\hat{s}) - B_0(m_Z^2 + \mathrm{i}\epsilon) \ , \tag{A.6}$$
$$\begin{aligned} C_Z(\hat{s}) \equiv C_Z(34) &= C_0(m_Z^2, 0, \hat{s}; m, m, m) \\ &= C_0(0, m_Z^2, \hat{s}; m, m, m) \ , \end{aligned} \tag{A.7}$$
$$\begin{aligned} D_Z(\hat{s}, \hat{u}) \equiv D_Z(123) &= D_0(0, 0, 0, m_Z^2, \hat{s}, \hat{u}; m, m, m, m) \\ &= D_Z(\hat{u}, \hat{s}) \ . \end{aligned} \tag{A.8}$$

The expressions

$$\begin{aligned} \tilde{F}(\hat{s}, \hat{t}, \hat{u}) \equiv\ & D_Z(\hat{s}, \hat{t}) + D_Z(\hat{s}, \hat{u}) \\ & + D_Z(\hat{u}, \hat{t}) \ , \end{aligned} \tag{A.9}$$
$$\begin{aligned} E(\hat{t}, \hat{u}) = E(\hat{u}, \hat{t}) \equiv\ & \hat{t} C_0(\hat{t}) + \hat{u} C_0(\hat{u}) + \hat{t}_1 C_Z(\hat{t}) \\ & + \hat{u}_1 C_Z(\hat{u}) - \hat{t}\hat{u} D_Z(\hat{t}, \hat{u}), \end{aligned} \tag{A.10}$$

appear naturally in the amplitudes below, where $\hat{s}_1 = \hat{s} - m_Z^2$, $\hat{t}_1 = \hat{t} - m_Z^2$, $\hat{u}_1 = \hat{u} - m_Z^2$.

The W-loop contribution to the helicity amplitudes may then be written as[4] [7,6]

$$F^W_{\lambda_1\lambda_2\lambda_3\lambda_4}(\hat{s}, \hat{t}, \hat{u}) \equiv \alpha^2 \ \frac{c_W}{s_W} A^W_{\lambda_1\lambda_2\lambda_3\lambda_4}(\hat{s}, \hat{t}, \hat{u}) \tag{A.11}$$

where

$$\begin{aligned} &A^W_{++++}(\hat{s}, \hat{t}, \hat{u}) \\ &= \frac{16\hat{s}_1}{\hat{s}} E(\hat{t}, \hat{u}) + 4\left[2\left(\hat{s} - 4m_W^2\right)\hat{s}_1 - m_W^2\left(m_Z^2 - 6m_W^2\right)\right] \\ &\times \tilde{F}\left(\hat{s}, \hat{t}, \hat{u}\right) + 2\left(\frac{m_Z^2}{m_W^2} - 6\right)\left\{\frac{\hat{t}\hat{u} + m_W^2(\hat{s} + \hat{s}_1)}{\hat{s}\hat{s}_1} E(\hat{t}, \hat{u})\right. \\ &- \frac{2m_W^2}{\hat{s}_1}\left[\hat{t}\hat{u} D_Z(\hat{t}, \hat{u}) + m_Z^2 C_0(\hat{s})\right] - \frac{(\hat{s} + m_Z^2)\hat{t}\hat{u}}{\hat{s}_1\hat{t}_1\hat{u}_1} \\ &- \frac{2m_W^2 m_Z^2 \hat{s}}{\hat{s}_1\hat{t}_1} C_Z(\hat{t}) + \left(\frac{2\hat{t} + \hat{s}}{\hat{s}_1} - \frac{m_Z^4\hat{s}}{\hat{s}_1\hat{t}_1^2}\right) B_Z(\hat{t}) \\ &\left. - \frac{2m_W^2 m_Z^2 \hat{s}}{\hat{s}_1\hat{u}_1} C_Z(\hat{u}) + \left(\frac{2\hat{u} + \hat{s}}{\hat{s}_1} - \frac{m_Z^4\hat{s}}{\hat{s}_1\hat{u}_1^2}\right) B_Z(\hat{u})\right\}, \end{aligned} \tag{A.12}$$

$$\begin{aligned} &A^W_{+++-}(\hat{s}, \hat{t}, \hat{u}) \\ &= 2\left(\frac{m_Z^2}{m_W^2} - 6\right)\left\{ - 2m_W^4 \tilde{F}(\hat{s}, \hat{t}, \hat{u}) - \frac{m_Z^2\hat{t}\hat{u}}{\hat{s}^2\hat{s}_1} E(\hat{t}, \hat{u})\right. \\ &+ m_W^2\left[\frac{(4m_Z^2 - \hat{s})\hat{t}\hat{u}}{\hat{s}\hat{s}_1} D_Z(\hat{t}, \hat{u}) - \frac{\hat{s}(\hat{u}^2 + \hat{t}^2)}{\hat{s}_1\hat{t}\hat{u}} C_0(\hat{s})\right. \\ &\left. - \frac{\hat{s}_1^2}{\hat{u}\hat{t}} C_Z(\hat{s})\right] + \frac{(\hat{s} + m_Z^2)\hat{t}\hat{u}}{\hat{s}_1\hat{t}_1\hat{u}_1} + m_W^2\left[\left(\frac{(m_Z^2\hat{u} - \hat{s}\hat{t})\hat{s}}{\hat{s}_1\hat{t}_1\hat{u}}\right.\right. \\ &\left.\left. + \frac{2m_Z^2\hat{u} - \hat{s}\hat{u}_1}{\hat{s}_1\hat{s}}\right) C_Z(\hat{t}) - \frac{(2m_Z^2\hat{u} + \hat{s}\hat{t})\hat{t}}{\hat{s}\hat{u}\hat{s}_1} C_0(\hat{t})\right. \\ &\left. - \frac{\hat{s}\hat{t}}{\hat{u}} D_Z(\hat{s}, \hat{t})\right] + m_W^2\left[\left(\frac{(m_Z^2\hat{t} - \hat{s}\hat{u})\hat{s}}{\hat{s}_1\hat{u}_1\hat{t}} + \frac{2m_Z^2\hat{t} - \hat{s}\hat{t}_1}{\hat{s}_1\hat{s}}\right)\right. \\ &\left. \times C_Z(\hat{u}) - \frac{(2m_Z^2\hat{t} + \hat{s}\hat{u})\hat{u}}{\hat{s}\hat{t}\hat{s}_1} C_0(\hat{u}) - \frac{\hat{s}\hat{u}}{\hat{t}} D_Z(\hat{s}, \hat{u})\right] \\ &\left. + \frac{m_Z^2(2\hat{t}_1 - \hat{s})\hat{u}\hat{t}}{\hat{s}\hat{s}_1\hat{t}_1^2} B_Z(\hat{t}) + \frac{m_Z^2(2\hat{u}_1 - \hat{s})\hat{u}\hat{t}}{\hat{s}\hat{s}_1\hat{u}_1^2} B_Z(\hat{u})\right\}, \end{aligned} \tag{A.13}$$

$$\begin{aligned} &A^W_{++-+}(\hat{s}, \hat{t}, \hat{u}) \\ &= 2\left(\frac{m_Z^2}{m_W^2} - 6\right)\left\{ - 2m_W^4 \tilde{F}(\hat{s}, \hat{t}, \hat{u}) + 1\right. \\ &- m_W^2\left[\frac{\hat{t}\hat{u}}{\hat{s}_1} D_Z(\hat{t}, \hat{u}) + \frac{\hat{s}(\hat{u}^2 + \hat{t}^2)}{\hat{s}_1\hat{t}\hat{u}} C_0(\hat{s}) + \frac{\hat{s}_1^2}{\hat{u}\hat{t}} C_Z(\hat{s})\right. \\ &+ \frac{\hat{t}\hat{s}}{\hat{u}} D_Z(\hat{s}, \hat{t}) + \frac{\hat{u}^2 + \hat{s}_1^2}{\hat{s}_1\hat{u}} C_0(\hat{t}) + \frac{\hat{t}\hat{t}_1}{\hat{s}_1\hat{u}} C_Z(\hat{t}) + \frac{\hat{s}\hat{u}}{\hat{t}} D_Z(\hat{s}, \hat{u}) \\ &\left.\left. + \frac{\hat{t}^2 + \hat{s}_1^2}{\hat{s}_1\hat{t}} C_0(\hat{u}) + \frac{\hat{u}\hat{u}_1}{\hat{s}_1\hat{t}} C_Z(\hat{u})\right]\right\}, \end{aligned} \tag{A.14}$$

$$\begin{aligned} &A^W_{++--}(\hat{s}, \hat{t}, \hat{u}) \\ &= 2\left(\frac{m_Z^2}{m_W^2} - 6\right)\{1 - 2m_W^4 \tilde{F}(\hat{s}, \hat{t}, \hat{u}) \\ &- \frac{m_W^2 m_Z^2}{\hat{s}\hat{s}_1}[E(\hat{u}, \hat{t}) + 2\hat{s} C_0(\hat{s})]\}, \end{aligned} \tag{A.15}$$

$$\begin{aligned} &A^W_{+-+-}(\hat{s}, \hat{t}, \hat{u}) = A^W_{+--+}(\hat{s}, \hat{u}, \hat{t}) \\ &= 16\frac{\hat{s}}{\hat{s}_1} E(\hat{s}, \hat{t}) + 4\left(\frac{2\hat{s}\hat{u}(\hat{u} - 4m_W^2)}{\hat{s}_1}\right. \\ &\left. - m_W^2(m_Z^2 - 6m_W^2)\right)\tilde{F}(\hat{s}, \hat{t}, \hat{u}) + 2\left(\frac{m_Z^2}{m_W^2} - 6\right) \\ &\times\left\{\left(\frac{\hat{s}\hat{t}}{\hat{u}^2} + \frac{2m_W^2}{\hat{u}}\right) E(\hat{s}, \hat{t}) - m_W^2\left[\frac{2\hat{s}\hat{t}}{\hat{u}} D_Z(\hat{s}, \hat{t})\right.\right. \\ &+ \frac{m_Z^2}{\hat{s}\hat{s}_1} E(\hat{u}, \hat{t}) + \frac{2m_Z^2(2\hat{t}_1 + \hat{s})}{\hat{s}_1\hat{t}_1} C_Z(\hat{t})\Big] + \frac{\hat{s}(\hat{s}_1 - \hat{t})}{\hat{s}_1\hat{u}} B_Z(\hat{s}) \\ &\left.\left. - \frac{\hat{s}\hat{t}(2\hat{s}_1\hat{t}_1 + \hat{t}\hat{u})}{\hat{s}_1\hat{u}\hat{t}_1^2} B_Z(\hat{t}) - \frac{\hat{s}\hat{t}}{\hat{s}_1\hat{t}_1}\right\}, \end{aligned} \tag{A.16}$$

$$A^W_{+---}(\hat{s}, \hat{t}, \hat{u}) = A^W_{+-++}(\hat{s}, \hat{u}, \hat{t})$$

[4] The easiest way to calculate this is to use a nonlinear gauge, as in [9], in which the couplings $\gamma W^{\pm}\phi^{\mp}$, $ZW^{\pm}\phi^{\mp}$ vanish. In such a gauge, the same propagator appears along the entire loop

$$
\begin{aligned}
&= \frac{8m_Z^2\hat{u}}{\hat{s}_1\hat{t}}\left[2E(\hat{s},\hat{u}) - \hat{t}(4m_W^2-\hat{t})\tilde{F}(\hat{s},\hat{t},\hat{u})\right]\\
&-2\left(\frac{m_Z^2}{m_W^2}-6\right)\left\{m_W^2\left[\left(\frac{\hat{s}\hat{u}}{\hat{t}}+2m_W^2\right)D_Z(\hat{s},\hat{u})\right.\right.\\
&+\left(\frac{\hat{s}\hat{t}}{\hat{u}}+2m_W^2\right)D_Z(\hat{s},\hat{t})+\left(\frac{\hat{t}\hat{u}}{\hat{s}_1}+2m_W^2\right)D_Z(\hat{t},\hat{u})\\
&+\frac{\hat{s}\hat{s}_1}{\hat{u}\hat{t}}C_0(\hat{s})+\frac{\hat{u}^2}{\hat{s}_1\hat{t}}C_0(\hat{u})+\frac{\hat{u}^2+\hat{s}_1^2}{\hat{s}_1\hat{u}}C_0(\hat{t})+\frac{\hat{u}^2+\hat{t}^2}{\hat{u}\hat{t}}C_Z(\hat{s})\\
&\left.+\frac{2m_Z^2\hat{t}^2+\hat{u}_1(\hat{t}\hat{t}_1+\hat{s}\hat{s}_1)}{\hat{s}_1\hat{u}_1\hat{t}}C_Z(\hat{u})+\frac{\hat{t}\hat{t}_1}{\hat{s}_1\hat{u}}C_Z(\hat{t})\right]\\
&\left.+\frac{m_Z^2\hat{t}\hat{u}}{\hat{s}_1\hat{u}_1^2}B_Z(\hat{u})-\frac{\hat{s}\hat{u}}{\hat{s}_1\hat{u}_1}\right\}, \qquad \text{(A.17)}
\end{aligned}
$$

$$
\begin{aligned}
&A^W_{+++0}(\hat{s},\hat{t},\hat{u})\\
&= p_t\sqrt{2}\,m_Z\left(\frac{m_Z^2}{m_W^2}-6\right)\left\{(\hat{t}-\hat{u})\left[\frac{3m_W^2}{\hat{s}_1}D_Z(\hat{t},\hat{u})\right.\right.\\
&-\frac{E(\hat{t},\hat{u})}{\hat{s}\hat{s}_1}+\frac{2m_W^2\hat{s}}{\hat{s}_1\hat{t}\hat{u}}C_0(\hat{s})+\left.\frac{2\hat{s}}{\hat{s}_1\hat{t}_1\hat{u}_1}\right]+m_W^2\left[\frac{\hat{s}}{\hat{u}}D_Z(\hat{s},\hat{t})\right.\\
&+\frac{2}{\hat{s}_1}C_0(\hat{t})+\left.\frac{2(2\hat{s}^2-\hat{t}_1^2)}{\hat{s}_1\hat{t}_1\hat{u}}C_Z(\hat{t})\right]+\frac{2(2\hat{t}_1\hat{t}+m_Z^2\hat{u})}{\hat{s}_1\hat{t}_1^2}B_Z(\hat{t})\\
&-m_W^2\left[\frac{\hat{s}}{\hat{t}}D_Z(\hat{s},\hat{u})+\frac{2}{\hat{s}_1}C_0(\hat{u})+\frac{2(2\hat{s}^2-\hat{u}_1^2)}{\hat{s}_1\hat{u}_1\hat{t}}C_Z(\hat{u})\right]\\
&\left.-\frac{2(2\hat{u}_1\hat{u}+m_Z^2\hat{t})}{\hat{s}_1\hat{u}_1^2}B_Z(\hat{u})\right\}, \qquad \text{(A.18)}
\end{aligned}
$$

$$
\begin{aligned}
&A^W_{++-0}(\hat{s},\hat{t},\hat{u})\\
&= p_t\sqrt{2}\,m_Z(m_Z^2-6m_W^2)\left\{\frac{(\hat{t}-\hat{u})}{\hat{s}_1}\left(D_Z(\hat{t},\hat{u})-\frac{2\hat{s}}{\hat{u}\hat{t}}C_0(\hat{s})\right)\right.\\
&-\frac{\hat{s}}{\hat{u}}D_Z(\hat{s},\hat{t})+\frac{2}{\hat{s}_1}C_0(\hat{t})-\frac{2\hat{t}_1}{\hat{s}_1\hat{u}}C_Z(\hat{t})+\frac{\hat{s}}{\hat{t}}D_Z(\hat{s},\hat{u})\\
&\left.-\frac{2}{\hat{s}_1}C_0(\hat{u})+\frac{2\hat{u}_1}{\hat{s}_1\hat{t}}C_Z(\hat{u})\right\}, \qquad \text{(A.19)}
\end{aligned}
$$

$$
\begin{aligned}
&A^W_{+-+0}(\hat{s},\hat{t},\hat{u}) = A^W_{+--0}(\hat{s},\hat{u},\hat{t})\\
&= p_t\sqrt{2}\left\{\frac{8m_Z\hat{s}}{\hat{s}_1}\left[(\hat{u}-4m_W^2)\tilde{F}(\hat{s},\hat{t},\hat{u})+\frac{2E(\hat{s},\hat{t})}{\hat{u}}\right]\right.\\
&+m_Z\left(\frac{m_Z^2}{m_W^2}-6\right)\left\{m_W^2\left[\frac{(\hat{t}-\hat{u})}{\hat{s}_1}D_Z(\hat{t},\hat{u})+\frac{\hat{s}}{\hat{t}}D_Z(\hat{s},\hat{u})\right.\right.\\
&\left.+\frac{3\hat{s}}{\hat{u}}D_Z(\hat{s},\hat{t})\right]+\frac{2m_W^2}{\hat{s}_1}\left[C_0(\hat{t})+C_0(\hat{u})-\frac{\hat{s}\hat{s}_1}{\hat{u}\hat{t}}C_0(\hat{s})\right.\\
&+\frac{\hat{u}_1}{\hat{t}}C_Z(\hat{u})+\frac{\hat{t}_1}{\hat{u}}C_Z(\hat{t})-\left.\frac{2\hat{u}}{\hat{t}_1}C_Z(\hat{t})\right]-\frac{\hat{s}}{u^2}E(\hat{s},\hat{t})\\
&\left.\left.+\frac{2\hat{s}}{\hat{s}_1\hat{u}}B_Z(\hat{s})-2\left(\frac{1}{\hat{u}}+\frac{m_Z^2\hat{u}}{\hat{s}_1\hat{t}_1^2}\right)B_Z(\hat{t})+\frac{2\hat{s}}{\hat{s}_1\hat{t}_1}\right\}\right\}, \qquad \text{(A.20)}
\end{aligned}
$$

where

$$
p_t = \sqrt{\frac{\hat{t}\hat{u}}{\hat{s}}}\ . \qquad \text{(A.21)}
$$

When comparing these results with those of [7], where helicity amplitudes are also given, we identify some discrepancies in (A.13, A.14, A.18, A.19, A.20) that are of minor importance, since the affected amplitudes are very small. In addition, there is a difference in sign for the longitudinal Z amplitudes, since [7] does not use the Jakob–Wick convention[5].

We next turn to the *fermion*-loop contribution. Writing the effective $Zf\bar{f}$ interaction as

$$
\mathcal{L}_{Zff} = -\mathrm{e}Z^\mu\bar{f}(\gamma_\mu g^Z_{Vf}-\gamma_\mu\gamma_5 g^Z_{Af})f, \qquad \text{(A.22)}
$$

we remark that, due to charge conjugation, only the vector coupling g^Z_{Vf} gives a nonvanishing contribution. For ordinary quarks and leptons, this is

$$
g^Z_{Vf} = \frac{t_3^f - 2Q_f s_W^2}{2s_W c_W}\ , \qquad \text{(A.23)}
$$

where t_3^f is the fermion third isospin component, and Q_f its charge. Denoting then the fermion mass as m_f, its contribution to the helicity amplitudes is written as [8]

$$
F^f_{\lambda_1\lambda_2\lambda_3\lambda_4}(\hat{s},\hat{t},\hat{u}) \equiv \alpha^2 Q_f^3 g^Z_{Vf} A^f_{\lambda_1\lambda_2\lambda_3\lambda_4}(\hat{s},\hat{t},\hat{u})\ . \qquad \text{(A.24)}
$$

For the presentation of the fermion-loop contribution, it is convenient to introduce the definitions

$$
x_f \equiv \frac{4m_f^2}{m_Z^2-6m_f^2} \qquad \text{(A.25)}
$$

and[6]

$$
\begin{aligned}
G_f(\hat{s},\hat{t},\hat{u}) &= \frac{(10m_f^2+m_Z^2)}{m_f^2}E(\hat{t},\hat{u})+2\hat{s}\\
&\times\left[4\hat{s}-10m_f^2-m_Z^2\right]\tilde{F}(\hat{s},\hat{t},\hat{u})\ , \qquad \text{(A.26)}
\end{aligned}
$$

which allow us to write [8]

$$
\begin{aligned}
A^f_{++++}(\hat{s},\hat{t},\hat{u}) &= x_f A^W_{++++}(\hat{s},\hat{t},\hat{u};\ m_W\to m_f)\\
&-\frac{x_f\hat{s}_1}{\hat{s}}G_f(\hat{s},\hat{t},\hat{u})\ , \qquad \text{(A.27)}
\end{aligned}
$$

$$
A^f_{+++-}(\hat{s},\hat{t},\hat{u}) = x_f A^W_{+++-}(\hat{s},\hat{t},\hat{u};\ m_W\to m_f)\ , \qquad \text{(A.28)}
$$

$$
A^f_{++-+}(\hat{s},\hat{t},\hat{u}) = x_f A^W_{++-+}(\hat{s},\hat{t},\hat{u};\ m_W\to m_f)\ , \qquad \text{(A.29)}
$$

$$
A^f_{++--}(\hat{s},\hat{t},\hat{u}) = x_f A^W_{++--}(\hat{s},\hat{t},\hat{u};\ m_W\to m_f)\ , \qquad \text{(A.30)}
$$

$$
\begin{aligned}
A^f_{+-+-}(\hat{s},\hat{t},\hat{u}) &= A^f_{+--+}(\hat{s},\hat{u},\hat{t})\\
&= x_f A^W_{+-+-}(\hat{s},\hat{t},\hat{u};m_W\to m_f)
\end{aligned}
$$

[5] Note also that the definitions of $\hat{t}$ and $\hat{u}$ used here and in [1,2] should be interchanged when they are compared with [7]

[6] The functions $E(\hat{t},\hat{u})$ and $\tilde{F}(\hat{s},\hat{t},\hat{u})$ are defined in (A.10) and (A.9), respectively, with $m = m_f$

$$-\frac{x_f \hat{s}}{\hat{s}_1} G_f(\hat{u},\hat{t},\hat{s}) \ , \tag{A.31}$$

$$\begin{aligned} A^f_{+---}(\hat{s},\hat{t},\hat{u}) &= A^f_{+-++}(\hat{s},\hat{u},\hat{t}) \\ &= x_f A^W_{+---}(\hat{s},\hat{t},\hat{u};\ m_W \to m_f) \\ &\quad -\frac{x_f \hat{u} m_Z^2}{\hat{s}_1 \hat{t}} G_f(\hat{t},\hat{s},\hat{u}), \end{aligned} \tag{A.32}$$

$$A^f_{+++0}(\hat{s},\hat{t},\hat{u}) = x_f A^W_{+++0}(\hat{s},\hat{t},\hat{u};\ m_W \to m_f) \ , \tag{A.33}$$

$$A^f_{++-0}(\hat{s},\hat{t},\hat{u}) = x_f A^W_{++-0}(\hat{s},\hat{t},\hat{u};\ m_W \to m_f) \ , \tag{A.34}$$

$$\begin{aligned} A^f_{+-+0}(\hat{s},\hat{t},\hat{u}) &= A^f_{+--0}(\hat{s},\hat{u},\hat{t}) \\ &= x_f A^W_{+-+0}(\hat{s},\hat{t},\hat{u};\ m_W \to m_f) \\ &\quad -\frac{x_f m_Z}{\hat{s}_1}\sqrt{\frac{2\hat{t}\hat{s}}{\hat{u}}} G_f(\hat{u},\hat{t},\hat{s}) \ . \end{aligned} \tag{A.35}$$

Finally, the contribution to the helicity amplitudes arising from a loop because of an *scalar* particle[7] of charge Q_S, mass m_S, and third isospin component t_3^S, is

$$F^S_{\lambda_1\lambda_2\lambda_3\lambda_4}(\hat{s},\hat{t},\hat{u}) \equiv \alpha^2 Q_S^3 g_S^Z A^S_{\lambda_1\lambda_2\lambda_3\lambda_4}(\hat{s},\hat{t},\hat{u}) \ , \tag{A.36}$$

where

$$g_S^Z = \frac{t_3^S - Q_S s_W^2}{s_W c_W} \ . \tag{A.37}$$

Using then the definitions

$$x_S = \frac{2m_S^2}{6m_S^2 - m_Z^2} \ , \tag{A.38}$$

$$G_S(\hat{s},\hat{t},\hat{u}) = 2E(\hat{t},\hat{u}) + \hat{s}(\hat{s} - 4m_S^2)\tilde{F}(\hat{s},\hat{t},\hat{u}) \ , \tag{A.39}$$

we obtain

$$\begin{aligned} A^S_{++++}(\hat{s},\hat{t},\hat{u}) &= x_S A^W_{++++}(\hat{s},\hat{t},\hat{u};\ m_W \to m_S) \\ &\quad -\frac{8x_S\hat{s}_1}{\hat{s}} G_S(\hat{s},\hat{t},\hat{u}) \ , \end{aligned} \tag{A.40}$$

$$A^S_{+++-}(\hat{s},\hat{t},\hat{u}) = x_S A^W_{+++-}(\hat{s},\hat{t},\hat{u};\ m_W \to m_S) \ , \tag{A.41}$$

$$A^S_{++-+}(\hat{s},\hat{t},\hat{u}) = x_S A^W_{++-+}(\hat{s},\hat{t},\hat{u};\ m_W \to m_S) \ , \tag{A.42}$$

$$A^S_{++--}(\hat{s},\hat{t},\hat{u}) = x_S A^W_{++--}(\hat{s},\hat{t},\hat{u};\ m_W \to m_S) \ , \tag{A.43}$$

$$\begin{aligned} A^S_{+-+-}(\hat{s},\hat{t},\hat{u}) &= A^S_{+--+}(\hat{s},\hat{u},\hat{t}) \\ &= x_S A^W_{+-+-}(\hat{s},\hat{t},\hat{u}; m_W \to m_S) \\ &\quad -\frac{8x_S\hat{s}}{\hat{s}_1} G_S(\hat{u},\hat{t},\hat{s}) \ , \end{aligned} \tag{A.44}$$

$$\begin{aligned} A^S_{+---}(\hat{s},\hat{t},\hat{u}) &= A^S_{+-++}(\hat{s},\hat{u},\hat{t}) \\ &= x_S A^W_{+---}(\hat{s},\hat{t},\hat{u};\ m_W \to m_S) \\ &\quad -\frac{8x_S\hat{u}m_Z^2}{\hat{s}_1\hat{t}} G_S(\hat{t},\hat{s},\hat{u}), \end{aligned} \tag{A.45}$$

[7] For example, an slepton

$$A^S_{+++0}(\hat{s},\hat{t},\hat{u}) = x_S A^W_{+++0}(\hat{s},\hat{t},\hat{u};\ m_W \to m_S) \ , \tag{A.46}$$

$$A^S_{++-0}(\hat{s},\hat{t},\hat{u}) = x_S A^W_{++-0}(\hat{s},\hat{t},\hat{u};\ m_W \to m_S) \ , \tag{A.47}$$

$$\begin{aligned} A^S_{+-+0}(\hat{s},\hat{t},\hat{u}) &= A^S_{+--0}(\hat{s},\hat{u},\hat{t}) \\ &= x_S A^W_{+-+0}(\hat{s},\hat{t},\hat{u};\ m_W \to m_S) \\ &\quad -\frac{8x_S m_Z}{\hat{s}_1}\sqrt{\frac{2\hat{t}\hat{s}}{\hat{u}}} G_S(\hat{u},\hat{t},\hat{s}) \ . \end{aligned} \tag{A.48}$$

Appendix B: the asymptotic $\gamma\gamma \to \gamma Z$ amplitudes in SM

At high energies, the one-loop functions simplify considerably. Such asymptotic expressions are very useful in elucidating the physical properties of the amplitudes at high energies, as can be seen from [1] for the $\gamma\gamma \to \gamma\gamma$ case. In this appendix, we therefore present the asymptotic expression for one-loop functions relevant for the $\gamma\gamma \to \gamma Z$ amplitudes.

Using thus the well-known asymptotic expression for the B_0 function of (A.4),

$$B_0(\hat{s}) \simeq \Delta + 2 - \ln\left(\frac{-\hat{s} - \mathrm{i}\epsilon}{\mu^2}\right) \ , \tag{B.1}$$

where Δ is the usual infinite term entering the calculation of the divergent integral [14], we obtain for the $B_Z(\hat{s})$ function defined in (A.6):

$$B_Z(\hat{s}) \simeq -\ln\left(\frac{-\hat{s} - \mathrm{i}\epsilon}{-m_Z^2 - \mathrm{i}\epsilon}\right) \ , \quad \text{for} \quad |\hat{s}| \gg (m^2,\ m_Z^2) \ . \tag{B.2}$$

For the $C_0(\hat{s})$ function defined in (A.5), a useful form is [15]:

$$C_0(\hat{s}) \simeq \frac{1}{2\hat{s}}\left[\ln\left(\frac{-\hat{s} - \mathrm{i}\epsilon}{m^2}\right)\right]^2 \ . \tag{B.3}$$

We next turn to $C_Z(\hat{s})$ and $D_Z(\hat{s},\hat{u})$ of (A.7, A.8), which also depend on m/m_Z. Simple asymptotic expressions are derived for them for arbitrary m/m_Z, using the results of [15]. To present them, we first introduce the quantity

$$a_Z \equiv \sqrt{1 - \frac{4m^2}{m_Z^2} + \mathrm{i}\epsilon}. \tag{B.4}$$

Then, for $|\hat{s}| \gg (m^2,\ m_Z^2)$,

$$\begin{aligned} C_Z(\hat{s}) \simeq \frac{1}{\hat{s}}\Bigg\{ & \frac{1}{2}\ln^2\left(\frac{-\hat{s} - \mathrm{i}\epsilon}{m^2}\right) + \frac{\pi^2}{2} - \frac{1}{2}\left[\ln\left(\frac{1+a_Z}{2}\right)\right. \\ & \left. -\ln\left(\frac{1-a_Z}{2}\right)\right]^2 + \mathrm{i}\pi\left[\ln\left(\frac{1+a_Z}{2}\right)\right. \\ & \left. -\ln\left(\frac{1-a_Z}{2}\right)\right] + O\left(\frac{1}{\hat{s}}\right)\Bigg\} \ , \end{aligned} \tag{B.5}$$

while for $(|\hat{s}|,\ |\hat{u}|) \gg (m^2,\ m_Z^2)$,

$$D_Z(\hat{s},\hat{u}) \simeq \frac{2}{\hat{s}\hat{u}}\Bigg\{ \ln\left(\frac{-\hat{s}-\mathrm{i}\epsilon}{m^2}\right)\ln\left(\frac{-\hat{u}-\mathrm{i}\epsilon}{m^2}\right) - \frac{1}{2}\left[\ln\left(\frac{1+a_Z}{2}\right) - \ln\left(\frac{1-a_Z}{2}\right)\right]^2 + \mathrm{i}\pi\left[\ln\left(\frac{1+a_Z}{2}\right) - \ln\left(\frac{1-a_Z}{2}\right)\right] + O\left(\frac{1}{\hat{s}}\ ,\ \frac{1}{\hat{u}}\right)\Bigg\}\ . \tag{B.6}$$

In all cases, the principal value of the logarithm, which has its cut along the negative real axis, is understood.

We next turn to the functions $\tilde{F}(\hat{s},\hat{t},\hat{u})$ and $E(\hat{t},\hat{u})$ defined in (A.9, A.10), which, together with $B_Z(\hat{s})$ (compare (B.2)), determine the high-energy behavior of the various $\gamma\gamma \to \gamma Z$ amplitudes. Using (B.5, B.6), they can be expressed for $(|\hat{s}|,\ |\hat{t}|,\ |\hat{u}|) \gg (m^2,\ m_Z^2)$ as

$$\tilde{F}(\hat{s},\hat{t},\hat{u}) \simeq \frac{2}{\hat{s}\hat{u}}\ln\left(\frac{-\hat{s}-\mathrm{i}\epsilon}{m^2}\right)\ln\left(\frac{-\hat{u}-\mathrm{i}\epsilon}{m^2}\right) + \frac{2}{\hat{s}\hat{t}}\ln\left(\frac{-\hat{s}-\mathrm{i}\epsilon}{m^2}\right)\ln\left(\frac{-\hat{t}-\mathrm{i}\epsilon}{m^2}\right) + \frac{2}{\hat{t}\hat{u}}\ln\left(\frac{-\hat{t}-\mathrm{i}\epsilon}{m^2}\right)\ln\left(\frac{-\hat{u}-\mathrm{i}\epsilon}{m^2}\right)\ , \tag{B.7}$$

$$E(\hat{t},\hat{u}) \simeq \pi^2 + \left[\ln\left(\frac{-\hat{t}-\mathrm{i}\epsilon}{m^2}\right) - \ln\left(\frac{-\hat{u}-\mathrm{i}\epsilon}{m^2}\right)\right]^2\ . \tag{B.8}$$

It is worth remarking that no a_Z term appears in (B.2), (B.7), or (B.8). This implies that the asymptotic $\gamma\gamma \to \gamma Z$ amplitudes do not depend on the ratio m_Z/m; this is as opposed to the situation for the asymptotic C_Z and D_Z functions.

The corresponding asymptotic expressions of the W-loop contributions, obtained from (A.12–A.20) for $(|\hat{s}|,\ |\hat{t}|,\ |\hat{u}|) \gg (m_W^2,\ m_Z^2)$ by neglecting terms of $O(m_W^2/\hat{s})$ but keeping terms of $O(m_W/\sqrt{s})$, are

$$A^W_{++++}(\hat{s},\hat{t},\hat{u}) \simeq 16E(\hat{t},\hat{u}) + 8\hat{s}^2\tilde{F}(\hat{s},\hat{t},\hat{u}) + 2\left(\frac{1}{c_W^2}-6\right) \times\left[\frac{\hat{t}\hat{u}}{\hat{s}^2}E(\hat{t},\hat{u}) - 1 + \frac{(\hat{t}-\hat{u})}{\hat{s}}[B_Z(\hat{t}) - B_Z(\hat{u})]\right]\ , \tag{B.9}$$

$$A^W_{+-+-}(\hat{s},\hat{t},\hat{u}) = A^W_{+--+}(\hat{s},\hat{u},\hat{t}) \simeq 16E(\hat{s},\hat{t}) + 8\hat{u}^2\tilde{F}(\hat{s},\hat{t},\hat{u}) + 2\left(\frac{1}{c_W^2}-6\right) \times\left[\frac{\hat{t}\hat{s}}{\hat{u}^2}E(\hat{s},\hat{t}) - 1 + \frac{(\hat{s}-\hat{t})}{\hat{u}}[B_Z(\hat{s}) - B_Z(\hat{t})]\right], \tag{B.10}$$

$$A^W_{+++0}(\hat{s},\hat{t},\hat{u}) = p_t\sqrt{2}\ m_Z\left(\frac{1}{c_W^2}-6\right)\Bigg[(\hat{t}-\hat{u})\left(-\frac{E(\hat{t},\hat{u})}{\hat{s}^2} + \frac{2}{\hat{t}\hat{u}}\right) + \frac{4}{\hat{s}}[B_Z(\hat{t}) - B_Z(\hat{u})]\Bigg]\ , \tag{B.11}$$

$$A^W_{+-+0}(\hat{s},\hat{t},\hat{u}) = A^W_{+--0}(\hat{s},\hat{u},\hat{t}) = p_t\sqrt{2}\ m_Z\Bigg\{8\hat{u}\tilde{F}(\hat{s},\hat{t},\hat{u}) + \frac{16}{\hat{u}}E(\hat{s},\hat{t}) + \left(\frac{1}{c_W^2}-6\right) \times\left[-\frac{\hat{s}}{\hat{u}^2}E(\hat{s},\hat{t}) + \frac{2}{\hat{u}}[B_Z(\hat{s}) - B_Z(\hat{t})] + \frac{2}{\hat{t}}\right]\Bigg\}, \tag{B.12}$$

$$A^W_{+++-}(\hat{s},\hat{t},\hat{u}) \simeq A^W_{++-+}(\hat{s},\hat{t},\hat{u}) \simeq A^W_{++--}(\hat{s},\hat{t},\hat{u}) \simeq A^W_{+-++}(\hat{s},\hat{t},\hat{u}) \simeq 2\left(\frac{1}{c_W^2}-6\right)\ , \tag{B.13}$$

$$A^W_{++-0} \simeq 0\ . \tag{B.14}$$

It is easy to see that at energies above 250 GeV, the Sudakov-like log-squared terms in (B.8, B.7) largely cancel out when substituted in these asymptotic amplitudes. Essentially, only the single-logarithm large imaginary terms remain, contributing to the dominant amplitudes $A^W_{++++}(\hat{s},\hat{t},\hat{u})$ and $A^W_{+-+-}(\hat{s},\hat{t},\hat{u}) = A^W_{+--+}(\hat{s},\hat{u},\hat{t})$. Almost negligible are the the amplitudes in (B.11, B.12), while the rest are even smaller.

Similar asymptotic expressions can also be obtained for the fermion-loop contributions appearing in (A.27–A.35), if one takes $(|\hat{s}|,\ |\hat{t}|,\ |\hat{u}|) \gg (m_f^2,\ m_Z^2)$ and uses (B.7, B.8). It turns out that at energies above 250 GeV, the fermion-loop contribution in the SM to the large imaginary parts of the amplitudes $F_{++++}(\hat{s},\hat{t},\hat{u})$ and $F_{+-+-}(\hat{s},\hat{t},\hat{u}) = F_{+--+}(\hat{s},\hat{u},\hat{t})$ is completely negligible. The W- and fermion-loop contributions are comparable only to the other very small amplitudes.

From Fig. 2 and Fig. 3, it can also be concluded that the real and imaginary contributions of a fermion or scalar loop are on an equal footing. As has been said already, the large imaginary contributions to $F_{++++}(\hat{s},\hat{t},\hat{u})$ and $F_{+-+-}(\hat{s},\hat{t},\hat{u}) = F_{+--+}(\hat{s},\hat{u},\hat{t})$ come from the dominant W loop only.

References

1. G.J. Gounaris, P.I. Porfyriadis, and F.M. Renard [hep-ph/9902230], Eur. Phys. Jour. C**9** (1999) 673.
2. G.J. Gounaris, P.I. Porfyriadis, and F.M. Renard [hep-ph/9812378], Phys. Lett. **B452** (1999) 76. Please notice that a factor i has been forgotten in front of the second term in equation (4) of the paper.
3. "Opportunities and requirements for experimentation at a very high energy e^+e^- collider", SLAC-329, 1928; *Proceedings of the Workshops on Japan Linear Collider*, KEK Reports, 90-2, 91-10, and 92-16; P.M. Zerwas, DESY 93-112, Aug. 1993; *Proceedings of the Workshop on e^+e^- Collisions at 500 GeV: The Physics Potential*, DESY 92-123 A, B, (1992), C (1993), D (1994), E (1997), edited by P. Zerwas; E. Accomando, et al., Phys. Rep. **C299** (1998) 299.

4. I.F. Ginzburg, G.L. Kotkin, V.G. Serbo, and V.I. Telnov, Nucl. Instr. and Meth. **205**, 47 (1983); I.F. Ginzburg, G.L. Kotkin, V.G. Serbo, S.L. Panfil, and V.I. Telnov, Nucl. Instr. and Meth. **219**, 5 (1984); J.H. Kühn, E. Mirkes and J. Steegborn, Z. f. Phys. **C57** (1993) 615
5. R. Brinkman, et al. [hep-ex/9707017]; V. Telnov [hep-ex/9802003, hep-ex/9805002]
6. E.W.N. Glover and A.G. Morgan, Z. f. Phys. **C60** (1993) 175; M. Bailargeon and F. Boudjema, Phys. Lett. **B272** (1991) 158; F.-X. Dong, X.-D. Jiang, and X.-J. Zhou, Phys. Rev. **D46** (1992) 5074; M.-z. Yang and X.j. Zhou, Phys. Rev. **D52** (1995) 5018.
7. G. Jikia and A. Tkabladze, Phys. Lett. **B332** (1994) 441; G. Jikia and A. Tkabladze, Phys. Lett. **B323** (1994) 453.
8. E.W.N. Glover and J.J. van der Bij, Nucl. Phys. **B313** (1989) 237; M.L. Lausen, K.O. Mikaelian, and M.A. Samuel, Phys. Rev. **D23** (1981) 2795
9. D.A. Dicus and C. Kao, Phys. Rev. **D49** (1994) 1265
10. G. Passarino and M. Veltman, Nucl. Phys. **B160** (1979) 151
11. S.Y. Choi, A. Djouadi, H. Dreiner, J. Kalinowski, and P.M. Zerwas [hep-ph/9806279], Eur. Phys. J. **C7** (1999) 123
12. G.J. van Oldenborgh and J.A.M. Vermaseren, Z. f. Phys. **C46** (1990) 425; G.J. van Oldenborgh, "FF: A package to evaluate one loop Feynman diagrams", Comput. Phys. Commun. **66** (1991) 1
13. G.J. Gounaris and G. Tsirigoti, Phys. Rev. **D56** (1997) 3030; ibid., **D58** (1998) 059901(E)
14. K. Hagiwara, S. Matsumoto, D. Haidt, and C.S. Kim, Z. f. Phys. **C64** (1995) 559
15. M. Roth and A. Denner, Nucl. Phys. **B479** (1996) 495 [hep-ph/9605420]; A. Denner and S. Dittmaier [hep-ph/9812411]